Power Systems Analysis Illustrated with MATLAB® and ETAP®

Hemchandra Madhusudan Shertukde

Power Systems Analysis Illustrated with MATLAB® and ETAP®

Power Systems Analysis Illustrated with MATLAB® and ETAP®

Hemchandra Madhusudan Shertukde

This book is dedicated to the arrival of our first granddaughter:

Arya J Bhakta

And to my entire family:

Rekha, Amola, Karan, Rohan and Jignesh

Contents

Foreword

Thomas Edison famously said, 'The doctor of the future will give no medicine, but will instruct his patient in the care of the human frame, in diet and in the cause and prevention of disease.'*

Power systems engineering is similar to the medical profession. Blood is a vital part of the human anatomy just as electricity is to modern civilization. We are most of the time unaware of the existence of either one of them; we rely on them for our daily functions and seldom pay attention to their importance until something goes wrong. Left unchecked, just as blood can carry the symptoms of a problem from the source to another point in the body, power systems issues originating in one area of the electrical network, such as power quality, coordination, arc flash, stability and so on, can manifest in areas least expected. Just like a doctor must diagnose a patient's health by analyzing bloodwork, it is crucial to diagnose the health of an electrical system by performing power systems analysis. Just as various bloodwork is necessary to understand the metrics in a body, power systems engineering has diverse analytical techniques and methods to pinpoint and understand the extent of the issue. A skilled engineer can then evaluate the impact of mitigation methods (medicine) prior to implementation, utilizing software tools such as ETAP to hone these diverse analytical methods. Power systems engineering has advanced such that Thomas Edison's famous quotation now holds true, where such software tools not only help us locate, diagnose, evaluate and mitigate the problems but also notify the power system's owner of imminent failure and recommend proactive action.

Most textbooks on power systems analysis discuss in great detail the techniques, methods, and theory and show the reader how analysis 'used' to be done. Power systems theory is indispensable, but knowledge on the application of that theory is essential in today's evolving power systems domain. Most students graduating learn this theory but fail to learn the application of the theory in a practical world. This book is exciting for me because Dr. Shertukde has delivered what power systems engineers and students of today need: the right balance between power systems theory and its engineering applications in the real world. Dr. Shertukde has successfully distilled 42 years of academic, industrial and leadership experience in the electrical engineering field in a clear, user-friendly yet focused manner. This is not another guidebook about power systems theory, as the use of ETAP and MATLAB® throughout the book, I am sure, will be refreshing and indispensable for the reader.

I feel honored and privileged to have this opportunity to write a foreword to Dr. Shertukde's book. I am sure it will find a wide audience and I cannot wait to add it as a vital reference book for power systems engineering and analysis.

Tanuj Khandelwal, CTO, ETAP
Irvine, California

---

* https://www.mindbodygreen.com/0-15699/why-functional-medicine-is-the-future-of-health.html.

Preface

In the everyday life of individuals, electrical power is a necessary commodity for survival. In the present day, having the light in one's home remain on is an absolute necessity. The power provided to residential, commercial or industrial locations is harnessed and delivered using several energy sources, including coal, hydel, nuclear, solar, wind, fuel cells and so on. The generated power needs to be transmitted over long distances to support the load requirements of customers. In order for this generation, transmission and distribution of power to be efficient, one needs to understand the proper design and analysis of a power system. Power flow needs to be reliable, of good quality and above all fault free. The improper design and analysis of power systems will result in the 'light not remaining on', so to speak, for everyone worldwide and will eventually lead to 'brown out' locally and 'blackout' globally.

I have taught power systems analysis (PSA) at the University of Hartford, Connecticut, for more than two decades and feel that the current books available on the market mainly provide detailed but unrelated concepts of PSA, making the basic understanding of the finer nuances of PSA difficult for senior undergraduate or junior graduate students. With the advances in computing and canned software for different applications (PSA is not an exception), the normal principles of PSA can be supplemented with state-of-the-art software such as the Electrical Transient Analysis Program (ETAP®). Many authors have tried their level best to explain these intriguing concepts in PSA using mainly theory without supplementing it with present-day examples of software used by the industry. This effort will alleviate that handicap and make the material in PSA more understandable to students. My studies at the Indian Institute of Technology, Kharagpur, West Bengal, India, involved broad and rounded coverage of the current topics in electrical engineering from 1970 to 1975. These topics were in controls and power. My fourth monograph was on one of the former topics in digital controls. This will be my fifth monograph on topics related to electrical engineering and my third in the electrical power engineering arena. For this book I have collaborated with Mr. Tanuj Khandelwal, CTO of Operation Technology, Inc. (OTI), Irvine, California, to incorporate the ETAP software into the material covered in this book to illustrate certain aspects of PSA, such as load flow analysis, short-circuit analysis and so on.
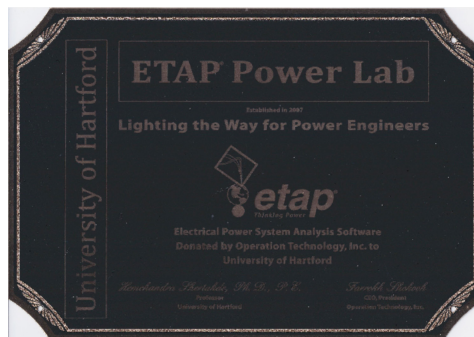
This is covered in the preamble to ETAP and is succinctly described in the foreword to this book by Mr. Khandelwal. I am grateful to him for providing this insight into the use of ETAP for PSA.

PSA has gone through many iterations, dealing with hand calculations, then aided by calculators, progressively evolving with the help of personal computers and now with miniaturized laptops and tablets with very high computing capabilities. My motivation to write a book on PSA started way back in 2006, when I received my first software grant ETAP from OTI to set up a power laboratory at the University of Hartford in 2007 (please see the preceding plaque). In 2007, OTI provided a software grant of 20 seats of ETAP to yours truly worth $265,000 with a continuing grant after 3 years of approximately $38,000 per year thereafter. This grant has continued to date and has been extremely useful in the instructions for the PSA course offered at the University of Hartford in the Samuel I. Ward Department of Electrical Engineering at the College of Engineering, Technology and Architecture (CETA).

Finally, I am grateful to Dr. Farrokh Shokooh, founder and CEO of OTI, for giving permission to incorporate ETAP into this book.

MATLAB® is a registered trademark of The MathWorks, Inc. For product information, please contact:

The MathWorks, Inc.
3 Apple Hill Drive
Natick, MA 01760-2098 USA
Tel: 508-647-7000
Fax: 508-647-7001
E-mail: info@mathworks.com
Web: www.mathworks.com

Acknowledgment

This is my third solo book in the field of electrical power engineering focused on power systems analysis. This effort truly reflects the rigor some of my professors at the Indian Institute of Technology (IIT) in Kharagpur, India, imbued in my study habits. I am grateful to all my professors in this area, namely Professor Mukhopadhyay, Professor Bandopadhyay and Professor Balaram Murthy. They taught me aspects of machine theory, switch gear and relays that form a complete core of pedagogy in the area of electrical power. As a professor myself I am proud to continue their legacy of lifelong teaching as I continue to complete my 31st year at the College of Engineering Technology and Architecture (CETA) in University of Hartford, West Hartford, Connecticut.

Author Biography

Hemchandra M. Shertukde, PhD, PE, IEEE- SM'92, is a Professor of Electrical Engineering at the University of Hartford, Connecticut, since 1996 and President of Diagnostic Devices Inc. Since 2008 he has been the Chair of the Task Force (TF) on DPV Grid Transformers, for IEEE-TC. The work of the TF resulted in a position paper which was accepted to be presented at the next IEEE-ICEEOT Conference in Chennai, March 3–5, 2016. He has served as the Chair of the WG.C.57.159 since 2011, which has compiled the User's Guide for the Understanding and Application of DPV Grid Transformers in the electrical grid, and was recently published by IEEE-Standards Association. He has written four books, two of which are *Transformers: Theory, Design and Practice with Practical Applications,* published by Verlag-Dr. Mueller, in August of 2010, and *Distributed Photovoltaic Grid Transformers,* published by CRC Press in March of 2014. Dr. Shertukde has published several transaction papers in *IEEE Transactions of Controls and Signal Processing* and proceeding papers in several international conferences. He holds a B.Tech from the Indian Institute of Technology Kharagpur, as well as an MS and PhD in electrical engineering with a specialty in controls and systems engineering from the University of Connecticut, Storrs. Currently, he is professor of electrical and computer engineering for the College of Engineering, Technology, and Architecture (CETA) at University of Hartford, Connecticut. He is also senior lecturer at the Yale School of Engineering and Applied Sciences (SEAS), New Haven, Connecticut. Dr. Shertukde is the principal inventor of two commercialized patents, 6,178,386 and 7,291,111. In 2017, Dr. Shertukde was a recipient of three IEEE awards viz: IEEE-SA/EAB award for contribution to standard association work and incorporating it effectively in education; IEEE-PES CT Chapter Outstanding Engineer Award for 2017 and IEEE-PES Transformer Committee Working Group Chair Award for WG C.57.159 User's Guide for DPV Grid Generating Systems. The IEEE-SA/EAB Award was re-awarded by IEEE-TC at the 100-year anniversary celebrations in March of 2018 in Pittsburgh, Pennsylvania.

Introduction to ETAP

ETAP is a full-spectrum analytical engineering software company specializing in the analysis, simulation, monitoring, control, optimization and automation of electrical power systems. ETAP software offers the best and most comprehensive suite of integrated power systems enterprise solutions, spanning modeling to operation.

- Offers a single connected platform with integrated applications
- Serves as an executable specification of the system under development
- Focuses on advanced power systems analytics
- Identifies root causes by the identification of operating problems
- Minimizes inadvertent outages caused by human error/equipment overload
- Offers optimization and business intelligence
- Provides design and operational insights
- Bridge the offline and online systems
- Reconstructs system conditions to check for user/operator actions
- Probes for alternative actions after the fact (*what-if analysis*)
- Facilities an ongoing learning process for the engineers and operators
- Enables data-driven decision-making and planning

ETAP is a fully graphical enterprise package that runs on the Microsoft® Windows® 2012, 2016, 7, 8, 8.1 and 10 operating systems. ETAP is the most comprehensive analysis tool available for the designing and testing of power systems. Using its standard offline simulation modules, ETAP can utilize real-time operating data for advanced monitoring, real-time simulation, optimization, energy management and high-speed intelligent load shedding.

ETAP has been designed and developed by OTI for engineers in Irvine to handle the diverse discipline of power systems for a broad spectrum of industries in one integrated package with multiple interface views, such as AC and DC networks, cable raceways, ground grid, geographic information systems (GISs), panels, arc flash, wind turbine generator (WTG), protective device coordination/selectivity and AC and DC control system diagrams.

ETAP allows you to easily create and edit graphical single-line diagrams (SLDs), underground cable raceway systems (UGSs), three-dimensional cable systems, advanced time-current coordination and selectivity plots, GIS schematics, as well as three-dimensional ground grid systems (GGSs). The program has been designed to incorporate the following four key concepts.

1. Virtual Reality Operation

The program operation emulates real electrical system operation as closely as possible. For example, when you open or close a circuit breaker, place an element out of service or change the operating status of the motors, the de-energized elements and sub-systems are indicated on the SLD in gray. ETAP incorporates

innovative concepts for determining protective device coordination directly from the SLD.

2. Total Integration of Data

ETAP combines the electrical, logical, mechanical and physical attributes of system elements in the same database. For example, a cable not only contains data representing its electrical properties and physical dimensions but also information indicating the raceways through which it is routed. Thus, the data for a single cable can be used for load flow or short-circuit analyses (which require electrical parameters and connections) as well as cable ampacity derating calculations (which require physical routing data). This integration of data provides consistency throughout the system and eliminates the need for multiple data entry for the same element, which can be a considerable time saver.

3. Simplicity in Data Entry

ETAP keeps track of the detailed data for each electrical apparatus. Data editors can speed up the data entry process by requiring the minimum data for a particular study. In order to achieve this, we have structured the property editors in the most logical manner for entering data for different types of analysis or design.

4. Quality Assurance

ETAP believes that a well-defined and effective quality assurance process that thrives on continuous improvement is the best vehicle to transform powerful ideas into powerful products. ETAP software meets the rigid standards for quality and safety established by U.S. and international standards bodies for nuclear facilities. In accordance with the ETAP Quality Assurance Program, all procedures and activities related to the quality of ETAP software are subject to audits. Qualified auditors periodically assess the program to detect any deviations from the complied standards and evaluate the effectiveness of the existing plans and procedures. Audit reports are properly documented and are subject to audits conducted by our nuclear clients and ISO 9001:2015 certification assessments. ETAP is on the supplier list of many nuclear facilities and Nuclear Procurement Issues Corporation (NUPIC) members. The ETAP Quality Assurance Program has undergone numerous audits since 1991. Our clients audit our program several times a year. For the past 2 years, the ETAP Quality Assurance Program has undergone audit assessments by the nuclear organizations.

ETAP products comply with the U.S. Code of Federal Regulations as well as other quality assurance standards. The ETAP Quality Assurance Program strictly enforces policies and specific procedures that ensure the reliability of all ETAP software. For nuclear/high-impact facilities, all releases of ETAP go through an intensive verification and validation (V&V) process throughout the revision life cycle. Verification is the process of determining whether or not the products of a given phase of the revision life cycle fulfill the requirements established during the previous phase. Validation is the process of evaluating software at the end of the revision life cycle to ensure compliance with software requirements.

The V&V method for ETAP is extensive, consisting of thousands of test cases that encompass each and every calculation module, user interface, persistence, reports, plots, library data and so on. The test cases include a comprehensive comparison of study results and system performance against hand calculations, field measurements, industry standards (ANSI/IEEE, IEC, UL, etc.) and other

established methods in order to ensure and verify the technical accuracy and performance stability of ETAP. The V&V process for the ETAP engineering libraries allows for 0% error in the library data based on published manufacturer data.

For further details of the different features available in the use of ETAP by Operations Technology Inc. for Power Systems Analysis are available at the URL: www.crcpress.com/9781498797214.

Benefits of Using ETAP for PSA

- Eliminate the man-hours and expense of internal software validation.
- Gain proof of software and libraries accuracy with minimal investment.
- Receive updated documentation on ongoing audits of ETAP.
- Operate your system with a virtual reality model concept.
- Gain more understanding of your system limitations.
- Manage system modifications in one integrated database.
- Have a team of experts for support.
- Avoid unnecessary system upgrade costs.

ETAP is a registered trademark of Operations Technology Inc.

Contact Information:

etap®
17 Goodyear
Irvine, CA 92618
United States of America

1

Introduction to Power Systems Analysis

1. Single-line diagram (SLD)
2. Components of an SLD
3. Equipment in an SLD
4. Generation, transmission and distribution parts of an SLD

Single-Line Diagram

Every power system in the world is represented by a single-line diagram (SLD; also known as a one-line diagram) consisting of a generator, several transmission lines, many different kinds of transformers and a motor as a load. Each of these components is represented by a single-phase circuit, assuming all the phases are identical. In general, many systems have three phases, although some can have two or more.

To properly and accurately analyze the power flowing through an SLD, one has to represent these components as their respective equivalent circuit. Let us strive to find these equivalent circuits, starting with the transformer. Any transformer is represented by its equivalent leakage reactance in series with an ideal transformer, as shown in Figure 1.1.

The second most important component is the generator, which can be represented by a voltage source in series with the synchronous reactance of the machine, as shown in Figure 1.2.

The third most important component of an SLD is the transmission line, represented by a π-circuit, which is a combination of passive elements, as shown in Figure 1.3.

Finally, the remaining component of an SLD is the motor as a rotating load; its equivalent circuit is shown in Figure 1.4.

Sometimes, the load can be a purely resistive circuit as a stationary load, shown as pure resistance in Figure 1.5.

Combining all the preceding individual equivalent circuits representing the respective equipment or components, we can evolve a working representation of an SLD, as shown in Figure 1.6.

The SLD shown in Figure 1.6 helps to transfer electrical power from the generating end to the load end. In stable conditions, power is delivered to the load reliably and without delay. However, faults in the SLD cause reliability problems, generating several delays, which can be detrimental to the efficient working of the power system. In order to analyze this loss in the performance of a power system, we need to conduct an analysis generally called a *power systems analysis* (PSA). To conduct this analysis properly, we need to have proper representations of all the components shown in Figure 1.6. This entails that each and every component needs to be studied thoroughly and correctly. This will be done component-wise below.
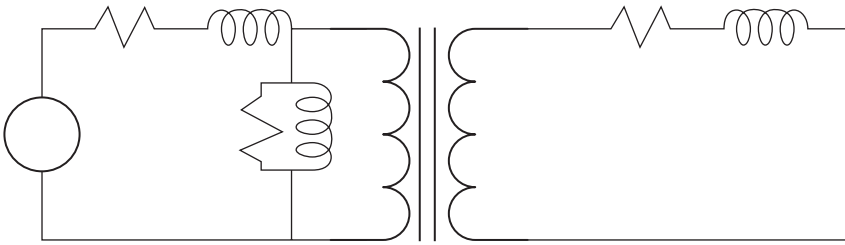
FIGURE 1.1
Equivalent circuit of a transformer.
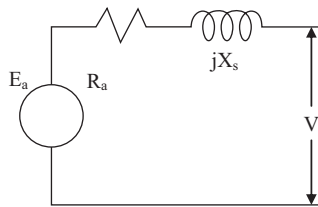
FIGURE 1.2
Equivalent circuit of a generator.
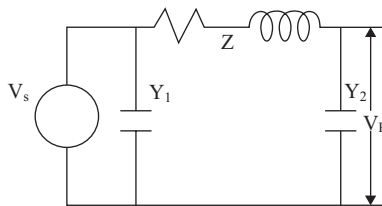
FIGURE 1.3
Equivalent circuit of a transmission line.
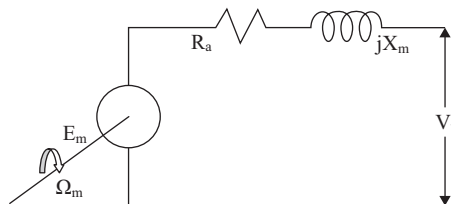
FIGURE 1.4
Equivalent circuit of a motor as a rotating load.

FIGURE 1.5
A pure resistive load.
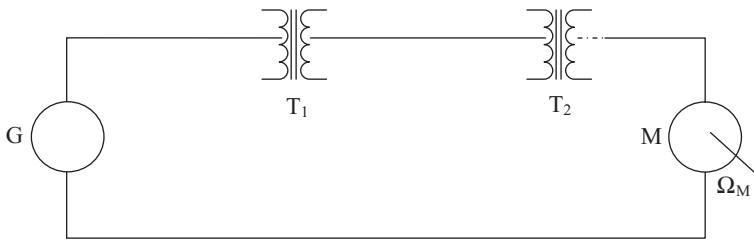
FIGURE 1.6
Working representation of an SLD.

Generation, Transmission, Distribution and Load Components of a Power System

Generation consists of a generator, which is generally a three-phase *synchronous machine*. This is a rotating electrical machine. The voltage rating of this component can reach as high as 33 kV.

Transmission consists of transmission lines, which are generally a set of three or four wires or conductors of a single strand or multiple strands. These are also along the way connected to different kinds and sets of transformers. The voltage rating of such components is very high. At present, they can reach 1500 kV.

Distribution consists of a set of three or four wires but at a lower voltage rating of up to 69 kV, reducing to 115 or 230 V single phase or 230 or 440 V three phase. In addition, it consists of either a rotating synchronous or asynchronous machine or a simple resistance connected at the load end to the distribution lines, along with suitably rated distribution transformers at the source end.

In addition to the these major components, the SLD has other components for the protection of the system, such as circuit breaker, switches, links and so on.

Example 1.1

A portion of the power system consists of two generators in parallel, as shown in Figure 1.7, connected to a step-up transformer that links them with a 230 kV transmission line. The detailed ratings for all components relevant to this example are as follows:

- Generator G_1: 10 MVA, with 12% reactance
- Generator G_2: 5 MVA, with 8% reactance
- Transformer T: 15 MVA, with 6% reactance
- Transmission line: $Z = (4 + j60)\ \Omega$, 230 kV
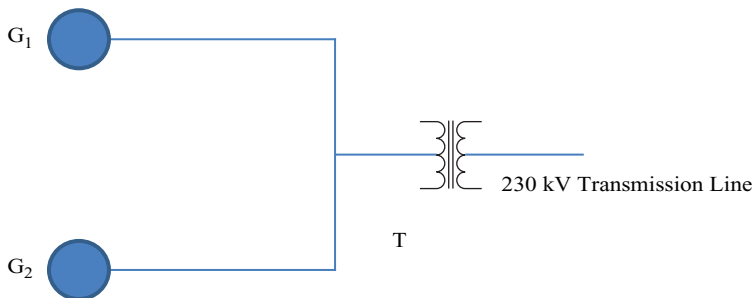
FIGURE 1.7
SLD of two generators connected to a transmission line via a transformer.

The percent reactances are computed on the basis of the individual ratings, respectively. Find the reactances and the impedance in percent with 15 MVA as the new base value.

SOLUTION 1.1

One needs to observe that the voltage is same for all the components in this example. Thus, the given and new voltage bases are the same. Using Equation A.38 as in Appendix A to obtain the pu values for all the components in the circuit, we have the following:

- Percent reactance of generator $G_1 = 12(15/10) = 18\%$
- Percent reactance of generator $G_2 = 8 (15/5) = 24\%$
- Percent reactance of transformer $T = 6(15/15) = 6\%$

Now we proceed to evaluate the transmission line as follows:

$$\text{Percent impedance} = Z = (4 + j60)(15 \times 10^6) / (230 \times 10^3)^2 \times 100$$

$$= (0.113 + j1.7)\%$$

Example 1.2

This example illustrates a four-bus electric power system, as shown in Figure 1.8. This example will also be illustrated using the latest ETAP® version of the software provided by Operation Technology, Inc. (OTI), Irvine, California.
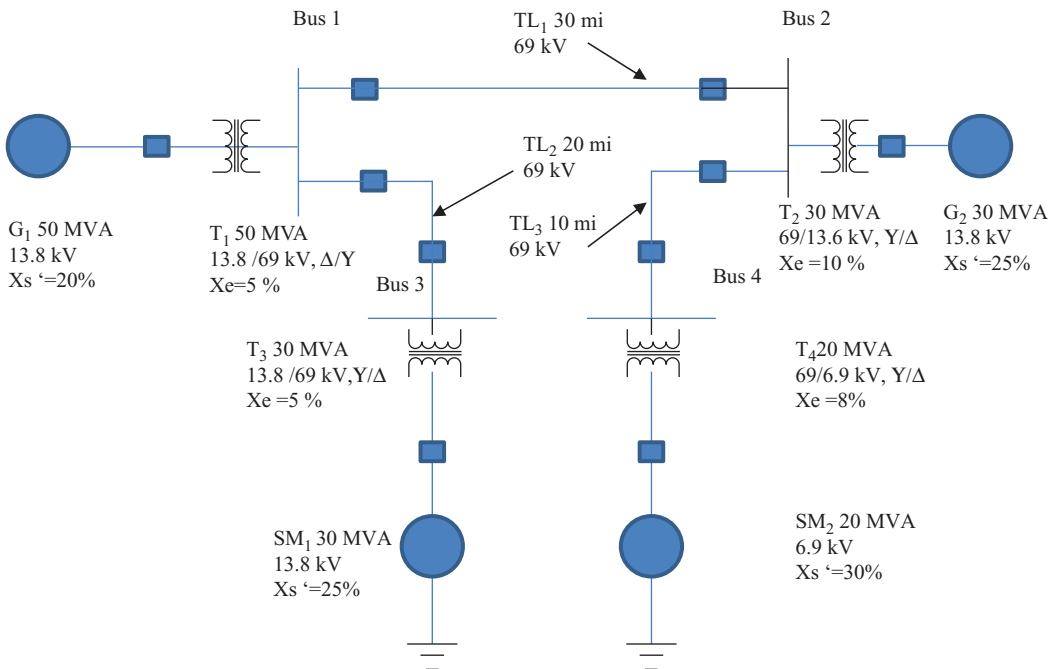
FIGURE 1.8
SLD of a four-bus electric power system.

1. Find the base impedance of the generator G_1 and determine the ohmic value of the transient reactance.
2. Find the base impedance of transformer T_4 at bus 4 referred to the low-voltage (LV) side of the transformer and evaluate the ohmic value of the leakage reactance on the LV side as the high-voltage (HV) side.

Generator G_1: 50 MVA, 13.8 kV, 20% transient reactance
Generator G_2: 30 MVA, 13.8 kV, 25% transient reactance
Transmission line MTL_1: 69 kV, 30 miles long
Transmission line TL_2: 69 kV, 20 miles long
Transmission line TL_3: 69 kV, 15 miles long
Synchronous machine SM_1: 30 MVA, 13.8 kV, 25% transient reactance
Synchronous machine SM_2: 20 MVA, 13.8 kV, 25% transient reactance
Transformer T_1: 50 MVA, 5% equivalent reactance, Delta/Wye, 13.8/69 kV
Transformer T_2: 30 MVA, 10% equivalent reactance, Wye/Delta, 69/13.8 kV
Transformer T_3: 30 MVA, 5% equivalent reactance, Wye/Delta, 69/13.8 kV
Transformer T_4: 20 MVA, 8% equivalent reactance, Wye/Delta, 69/6.9 kV
These components are configured in Figure 1.8.

SOLUTION 1.2

1. The base impedance of generator G_1 is given by

$$Z_{BG} = \frac{(13.8)^2}{50} = 3.81\,\Omega$$

Therefore,

$$X'_G = (\mathrm{pu}X')Z_{BG} = \left(\frac{20}{100}\right)(3.81) = 0.762\,\Omega$$

2. On examining the circuit SLD, one realizes that the LV rating of transformer T_4 is 6.9 kV. Hence, the base impedance of T_4 on the LV side is given by

$$Z_{BL} = \frac{(6.9)^2}{20} = 2.381\,\Omega$$

Thus,

$$X_{eqLV} = (\mathrm{pu}X_{eq})Z_{BL} = (0.08)(2.381) = 0.19\,\Omega$$

Knowing the turns ratio of transformer T_4 is $a = 10 = 69/6.9$, we have

$$X_{eqHV} = a^2 X_{eqLV} = \left(\frac{69}{6.9}\right)^2 (0.19) = 19\,\Omega$$

Example 1.3

Referring to Example 1.2 and the SLD in Figure 1.8, using all the same component details, determine the pu values of the reactances of generator G_1 and transformer T_4. Use a reference base as 100 MVA at 69 kV.

SOLUTION

In this case, referring to Figure 1.8, the reference voltage selection of 69 kV is the transmission line voltage. With this we can proceed with the evaluation of the pu values of the reactances posed in the problem statement as follows:

Generator G_1: If we examine the SLD in Figure 1.8, this generator is on the LV side of transformer T_1, so the reference voltage to be used for the conversion of the transient reactance of G_1 is 13.8 kV. Thus, using Equation A.38 in Appendix A, we have

$$\text{pu } X'_{sr} = \left(\frac{20}{100}\right)\left(\frac{13.8}{13.8}\right)^2\left(\frac{100}{50}\right) = 0.4$$

It is imperative to note here that this pu value is larger than the original or old value by a factor of 2. To recover the original or old value of this reactance, it is necessary to work with the reference base impedance on the LV side of G_1.

Thus,

$$Z_{BL} = \frac{(13.8)^2}{100} = 1.9\,\Omega$$

which yields $X'_s = (0.4)Z_{BL} = 0.762\,\Omega$, as before, and further yields the pu value of the equivalent reactance of T_4 as follows:

$$\text{pu } X_e = \left(\frac{8}{100}\right)\left(\frac{69}{69}\right)^2\left(\frac{100}{20}\right) = 0.4$$

As seen in Example 1.2 before.

2

Electrical Machines

2.1 Electrical Machines

These are the rotating machines that are part of the electrical machine domain.

2.1.1 Synchronous Machines

When a rotating machine speed is in synch with the power frequency of the applied signal, the appropriate speed of the shaft is given by the following equation:

$$n_s = \frac{120f}{p} \tag{2.1}$$

where:
  f is the frequency of the applied signal
  p is the number of poles of the machine initiating the magnetic flux
  n_s is the synchronous speed

The general Faraday's law is applied here as follows to the induced electromotive force (EMF) *e*, as in Equation 2.2 and illustrated in Figure 2.1.

$$e = \frac{d}{dt}(N\varphi)$$

$$= N\frac{d\varphi}{dt} + \varphi\frac{dN}{dt} \tag{2.2}$$

where:
  N is the number of turns in the rotor circuit
  Φ is the magnetic flux per pole created by the stator

As the rotor turns, the turns in the rotor circuit cut the spatially stationary magnetic flux, as shown in Figure 2.1 Thus, in Equation 2.2 for rotating machines, the first term is negligible, while the second term contributes to the effect caused by the rotating conductors and their cutting of the magnetic flux, thus resulting in the induced EMF. However, it is necessary for there to be an air gap between the stator's and rotor's magnetic circuits to cause the eventual rotating motion in the case of both the generator and motor actions of the synchronous machine, as is required of all rotating machines.
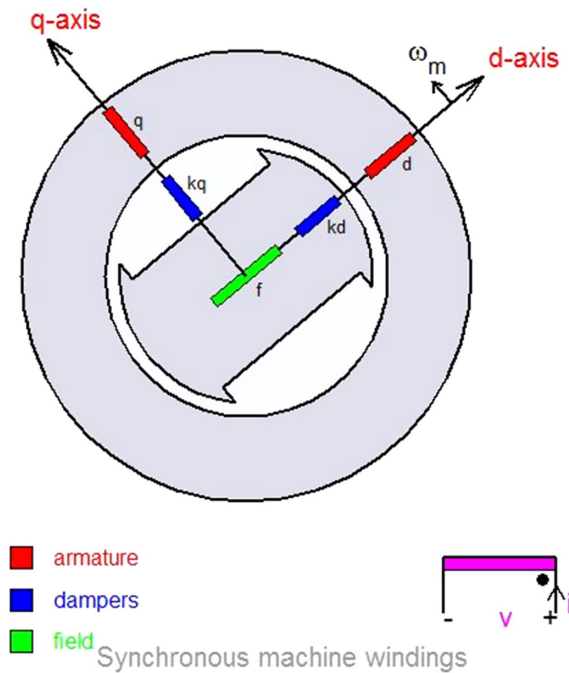
FIGURE 2.1
d-q model of the synchronous machine.

Because of the asymmetry of the synchronous machine created by rotor saliency and field excitation, the corresponding d-q model must use the rotor coordinates as a frame of reference. Details of the modeling are shown in Figure 2.1.

2.1.2 Asynchronous Machines

As discussed in Section 2.1.1, when the speed of an electrical machine is higher or lower than the synchronous speed, it is called an *asynchronous machine*. So, say we have a two-pole synchronous machine operating at a signal frequency of 60 c/s, with a synchronous speed of $n_s = 3600$ rpm, then an asynchronous machine operating at a slip s of 3%, will have a speed of $n = 3492$ rpm, as given by Equation 2.3.

$$n = n_s(1-s) \tag{2.3}$$

where n_s is the synchronous speed as given by Equation 2.1.

This concept of *slip* (*s*) will be studied in detail in this chapter as an important factor that defines the operation of an asynchronous machine. It means that the rotor 'slips' behind or ahead of the rotating stator magnetic field when slip *s* is positive or negative, respectively. In the scope of this book, the main emphasis will be on asynchronous machines operating as motors—popularly called *induction motors* (IMs) or *squirrel cage* IMs. The squirrel cage is the shape of the rotor conductors short-circuited on themselves. This action is shown in Figure 2.2.

All the preceding actions are described succinctly in Chapter 4 on generalized machine theory using d-q axis modeling.
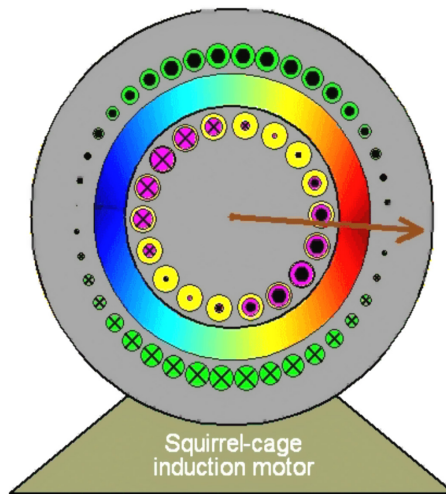
FIGURE 2.2
Squirrel cage IM.

2.1.3 Transformers

In Equation 2.2, when the first term is predominant and the second term is ignored since the machine components are stationary, the resulting machine with no air gap in the magnetic circuit is called a transformer.

Transformers are a vital part of power systems. Generally, seven to eight transformers are configured at strategically placed locations in the single-line diagram (SLD) of a power system, as follows:

- Generating point: generator step-up (GSU) transformer
- Receiving station point: receiving station (RS) transformer
- Substation point; substation transformer (ST)
- Distribution point: distribution station transformer (DST)
- Load point: where smaller-size transformers are connected to the load

Transformers thus form a major set of components in a single motor-generator system. This ratio of transformers to the motor-generator set is close to 10:1. The analysis of transformer theory can be easily understood by referring to [1]. The salient features of distributed photovoltaic grid transformers (DPV-GTs) are summarized in the following section.

2.2 Distributed Photovoltaic Grid Power Transformers [2]

2.2.1 Introduction

The increase in oil prices over the past few years has encouraged scientists, engineers and economists to look for alternative energy sources, one of which is the sun, whose abundant energy can be harnessed into reusable electric energy to supplement and

eventually be a major factor in overall energy generation, transmission and delivery to customers.

Wind energy, solar energy, and ocean wave energy have recently become notable players in this exchange. While penetration of alternate energy is the most important aspect of sustaining these alternative energies, considerable research and development work has been dedicated to the ancillary equipment needed for such energies to be efficiently delivered to the end user.

DPV-GTs, which convert solar energy, are gradually increasing in number in the field due to the recent focus on renewable energy sources. These transformers are primarily used as step-up transformers but can be used as step-down transformers as well. In the case of photovoltaic (PV) solar power, electrical power is generated by converting solar radiation into direct current (DC) electricity using semiconductors that exhibit the PV effect. PV power generation employs solar panels comprising a number of cells containing PV material.

The DC energy is then converted to one- or three-phase alternating current (AC) power using an inverter. The inverter is subsequently connected to a DPV-GT. This DPV-GT is further connected to a bus that can feed a suitable load. Figure 2.3 illustrates the process of converting energy from solar radiation into usable electrical power.

Currently, there are a variety of available industry standards that address many of these design, operation and maintenance aspects. Some of the key aspects to be considered are as follows.

2.2.2 Voltage Flicker and Variation [3]

Solar transformers operate at a steady voltage, with the rated voltage controlled by inverters. Therefore, voltage and load fluctuations are considerably reduced. The voltage variation is generally in the range of ±5% of the nominal voltage rating. Thus, standard design
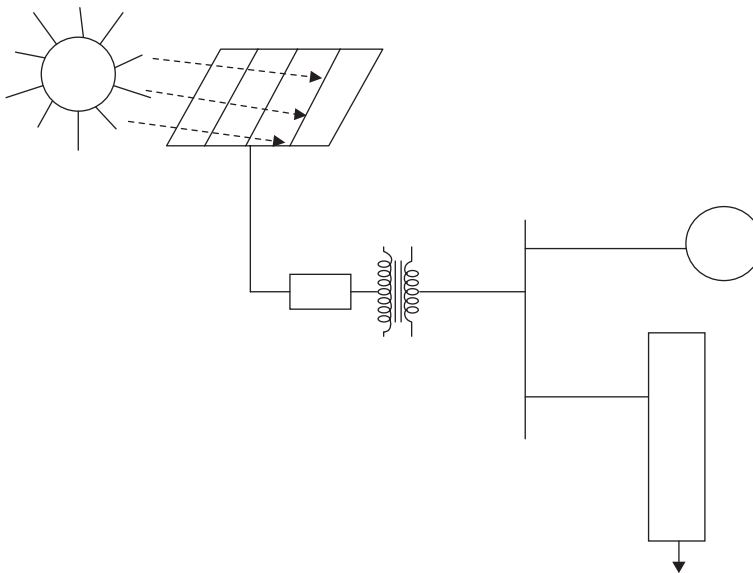
FIGURE 2.3
Typical one-line diagram with the solar panel connected to an inverter, which is in turn connected to a DPV-GT, a bus and further down to a load.

TABLE 2.1

Low-Voltage System Classification and Distortion Limits

	Special Applications[a]	General System	Dedicated System[b]
Notch Depth	10%	20%	50%
THD (Voltage)	3%	5%	10%
Notch Area (A_N)[c]	16,400	22,800	36,500

Source: Adapted and reprinted with permission from IEEE. © IEEE 1992. All rights reserved.
Note: The value A_N for other than 480 V systems should he multiplied by V/480.
[a] Special applications include hospitals and airports.
[b] A dedicated system is exclusively dedicated to the converter load.
[c] In volt-microseconds at rated voltage and current.

considerations for transformer windings are readily applied from experience. IEEE 519-92 [3] (Table 2.1) establishes limits for the allowable commutation notch depth introduced by power converters at critical points of the power system, normally coincident with transformer locations.

Load Tap Changer (LTC) control issues need to be addressed. Some LTCs are suitable to bidirectional power flow, but not all of them.

2.2.3 Harmonics and Waveform Distortion [3]

A solar inverter system's typical harmonic content is less than 5% (the threshold for normal service conditions), which has almost no impact on the system. The lower harmonic profile is because there are no generators or switching and protective controls such as those found on wind turbines.

IEEE C57.129 [4] sufficiently describes the requirements of the system designer to provide information on the harmonic content and the current waveform, including cases where there is more than one valve winding on a core leg.

IEEE C57.129 and C57.18.10 [5] use a definition of kVA rating based only on the fundamental frequency; additional losses due to the harmonic content are taken into account during the heat-run test.

IEEE 519-92 establishes limits for allowable harmonics levels in power systems. Table 2.2 shows the current distortion limits for general distribution systems (120–69,000 V) as a function of the short-circuit ratio and the harmonics order.

In case there is significant harmonic content in the DPV-GT, please refer to C57.110 [6], which is an IEEE Recommended Practice to establish a transformer's capability when supplying non-sinusoidal load current. Because of today's inverter practices, the harmonics generated from DC to AC conversion may be minimal, but they need to be included in the customer specifications so that transformer designers can take into account the additional losses due to harmonics in their transformer cooling designs.

2.2.4 Frequency Variation [7]

Since the frequency variation can come from the network only, there is no difference in design or manufacture from a 'standard' power transformer.

2.2.5 Power Factor (PF) Variation [7]

No significant differences from 'standard' power factor practices are expected.

TABLE 2.2

Current Distortion Limits for General Distribution Systems (120–69,000 V)

	Maximum Harmonic Current Distortion in Percent of I_L					
	Individual Harmonic Order (Odd Harmonics)					
I_{sc}/I_L	<11	$11 \le h < 17$	$17 \le h < 23$	$23 \le h < 35$	$35 \le h$	TDD
< 20[a]	4.0	2.0	1.5	0.6	0.3	5.0
20 < 50	7.0	3.5	2.5	1.0	0.5	8.0
50 < 100	10.0	4.5	4.0	1.5	0.7	12.0
100 < 1000	12.0	5.5	5.0	2.0	1.0	15.0
>1000	15.0	7.0	6.0	2.5	14	20.0

Source: Adapted and reprinted with permission from IEEE. © IEEE 1992. All rights reserved.
Notes: Even harmonics are limited to 25% of the odd harmonic limits.
Current distortions that result in a DC offset (e.g., half-wave converters) are not allowed.
[a] All power generation equipment is limited to these values of current distortion, regardless of actual I_{sc}/I_L, where I_{sc} = maximum short-circuit current at PCC and I_L = maximum demand load current (fundamental frequency component) at PCC.

IEEE C57.110 (§5.3 Power factor correction equipment): Power factor correction equipment is frequently installed to decrease utility costs. Care should be taken when this is done, since the current amplification in the circuit due to resonance at certain frequencies can be quite high. In addition, the inductance that is reduced in the circuit generally allows higher harmonic currents in the system. Harmonic heating effects from these conditions may be damaging to transformers and other equipment. The additional losses produced may also increase utility costs due to increased wattage requirements, even though the load power factor is improved.

2.2.6 Safety and Protection Related to the Public [7]

If residential and industrial (non-distributed) PV systems are addressed the specific safety requirements may be different from those power transformers, especially when it comes to residential applications.

IEEE C57.129: The converter transformer pollution aspects are extremely important and shall be accurately defined, so that proper external insulation (particularly bushings) may be provided.

2.2.7 Islanding [7]

In these conditions, when the system is functioning but not connected to a *high-inertia short-circuit capacity* network, then the system could be less stable and subject to frequency variations, but no significant differences from 'standard' transformers are expected.

2.2.8 Relay Protection [7]

The study of relay protection for DPV-GTs is extremely important given that such transformers operate with inverter circuits between the actual alternative energy source and the eventual connection to such transformers.

2.2.9 DC Bias [3]

IEEE C57.110 (§4.1.4 DC components of load current): Harmonic load currents are frequently accompanied by a DC component in the load current. The DC component of a load current will increase the transformer core loss slightly but will increase the magnetizing current and audible sound level more substantially. Relatively small DC components (up to the RMS magnitude of the transformer excitation current at the rated voltage) are expected to have no effect on the load-carrying capability of a transformer determined by this recommended practice. Higher DC load current components may adversely affect transformer capability and should be avoided.

Saturation of transformer core due to DC bias: One of the most important parameters to determine how much DC current will saturate the core is the core construction (three-phase three-limb, three-phase five-limb or single-phase cores). So, transformer manufacturers should gather data on possible DC bias currents before they finalize their designs. The saturation of the core is an important parameter to watch because of the possibility of ferro-resonance, in the case of cable-connected pad-mounted transformers, due to possible resonance between the non-linear self-inductance of the transformer and other capacitances connected in the system, such as the cable capacitance and filter capacitance of the inverter under saturation due to DC bias.

2.2.10 Thermocycling (Loading) [7]

In most geographical locations in the United States, solar power facilities experience steady-state loading when the inverters are operating. When the sun comes out, there is a dampened reaction process and the load on the transformer is more constant. The entire process is controlled by the insolation number in a particular location. The no-load operation of such transformers is completely controlled by a different set of parameters.

Nominal loading average: Solar power systems typically operate very close to their rated loads. Since the load variation from the rated value is appreciably low, the operation of transformers is not so adversely affected as to cause the deterioration of parameters that guide the insulation coordination of the core coil structure. Thus, forces experienced by the primary and secondary windings are not out of the ordinary, alleviating problems that may occur in the design of the mechanical structure.

Note on no-load operation: PV system transformers are subject to long-term no-load operation conditions, at least at night. This might have an impact on loss capitalization, which customers usually take into account, but also on the transformer design.

The storage battery's interaction with the transformer in a PV system may control the load consistency and alleviate the perceived problems.

The IEEE C57.129 standard requires a detailed thermal study if the transformer or some of the terminals operate above rated capacity. Standard power transformer loading tables *should not* be used for loading determination because of the effect of the harmonic currents and DC bias on the valve windings (for the high-voltage direct current (HVDC) converter transformers).

Even with the loss correction addressing the harmonic content during the heat run, the hot spot temperature may not be representative of the real conditions due to the nature of the harmonic current distribution in the winding and how it differs during the heat run. An 'extended load run with overload' is recommended by the CIGRE Joint Task Force 12/14.10-01 for HVDC converter transformers.

2.2.11 Power Quality [7]

Power quality aspects are generally addressed in other chapters of this book, although very clear emphasis is given to the preceding salient items.

2.2.12 Low-Voltage Fault Ride-Through

Fault ride-through has yet to be defined for solar power systems; this could be because it is easier to quickly turn solar power systems on and off.

2.2.13 Power Storage [7]

Battery storage impact will depend on the kind of system the DPV-GT is serving in a particular geographic environment.

2.2.14 Voltage Transients and Insulation Coordination [4]

Generator step-up duty: With solar transformers, step-up duty is required, but without the problems associated with over-voltages caused by unloaded generators. The inverter converts DC input from the PV array and provides AC voltage to the transformer, giving a steady and smooth transition, with no over-voltage caused by unloaded circuits. All general installations covered under this application pay much attention in their system considerations to over-voltage conditions. This problem is addressed by providing an *automatic gain control* scheme to the inverter circuit configuration.

The IEEE C57.129 standard provides specific recommendations on the insulation test levels for converter transformers. The development of a similar recommendation would be appropriate for the insulation test levels and procedures required to warrantee the reliability of the transformers in the PV application.

2.2.15 Magnetic Inrush Current [7]

Transformers experience a high current inrush when energized from a de-energized state. The inrush current is typically several times the rated current. The magnitude of the inrush current is determined by a variety of factors defined by the transformer design. The inrush current, when compared as a multiple of the rated current, is generally much higher when the energization takes place from the LV side. That is due to the fact that the LV winding is generally the winding that is closest to the core and therefore has a lower air-core reactance.

Since the inrush current is several times the rated current, each inrush event creates mechanical stresses within the transformer. Frequent energization from a de-energized state should be avoided since it wears down the transformer faster than normal. This should be a consideration for the operators of DPV step-up transformers, since they may wish to save energy by shutting down the transformers during the night. Such practices can shorten the transformer's life expectancy.

2.2.16 Eddy Current and Stray Losses [8]

Eddy currents and stray losses are present in every transformer. The primary stray and eddy losses are due to the 60 Hz fundamental frequency currents. These loss components

increase with the square of the frequency and the square of the magnitude of the eddy currents. If the inverter feeding the power into the step-up transformer is producing more than the standard level of harmonics, then the stray and eddy losses will increase. The effect of the increase in load loss on efficiency is not typically a concern. Of much greater concern is the increased hot spot temperature in the windings and hot spots in metallic parts that can reduce the transformer life. A special design transformer can compensate for the higher stray and eddy losses. Also, a larger than necessary kVA transformer can be selected to compensate for the higher operating temperatures. However, these concerns about increasing eddy current loss are generally mitigated since harmonics are less than 1%.

IEEE C57.129: The user shall clearly indicate the method to be used for evaluating the guaranteed load losses. The harmonic spectrum to be used for load loss evaluation shall be clearly identified. This spectrum may be different from the one specified for the temperature rise tests; the latter represents the worst-case operating conditions. A harmonic correction is added to the measured sinusoidal load losses as part of the calculation of the appropriate total loss value for the temperature rise test. The procedure to determine the total load losses is described in the standard.

2.2.17 Design Considerations: Inside/Outside Windings [4]

The design considerations for windings are dependent on the issues in the previous items, as shown in Figure 2.4. The design considerations to meet the special requirements depend on the manufacturer's construction, kVA size, voltage and other factors. Since inverter technology limits the size of the inverter, there may be multiple inverters at each solar station. Some users should consider having multiple LV windings in a single transformer, with each LV winding connected to an inverter. Design considerations such as impedance and short circuits cause multiple LV windings, creating a much more complex transformer. Additional complexity will increase cost and reduce the availability of the transformer. It is advisable to keep a transformer as simple as practical so that it can be mass produced and can be built by as many manufacturers as feasible.

In many cases, the limit of the kVA on the inverter circuits forces some of the designs to incorporate LV windings outside the HV windings. This enables easier connections to facilitate the paralleling of circuits to achieve a higher kVA rating for the entire transformer under consideration. This helps to alleviate some of the problems faced due to the constraints.

2.2.18 Special Test Considerations [4]

IEEE C57.129: Extended load run with overload; other power testing concepts and methodologies; specifics for the transformers used with voltage source converters. In addition to tests, a design review is recommended.

2.2.19 Special Design Considerations

Solar power systems use inverters to convert DC to AC. Since the largest practical inverter size to date is about 500 kVA, designers are building 1000 kVA transformers by placing two inverter-connected windings in one transformer. In this way the transformer has to have two separate windings to accept completely separate inputs. Design issues also stem from running cables long distances to convert from DC to AC.
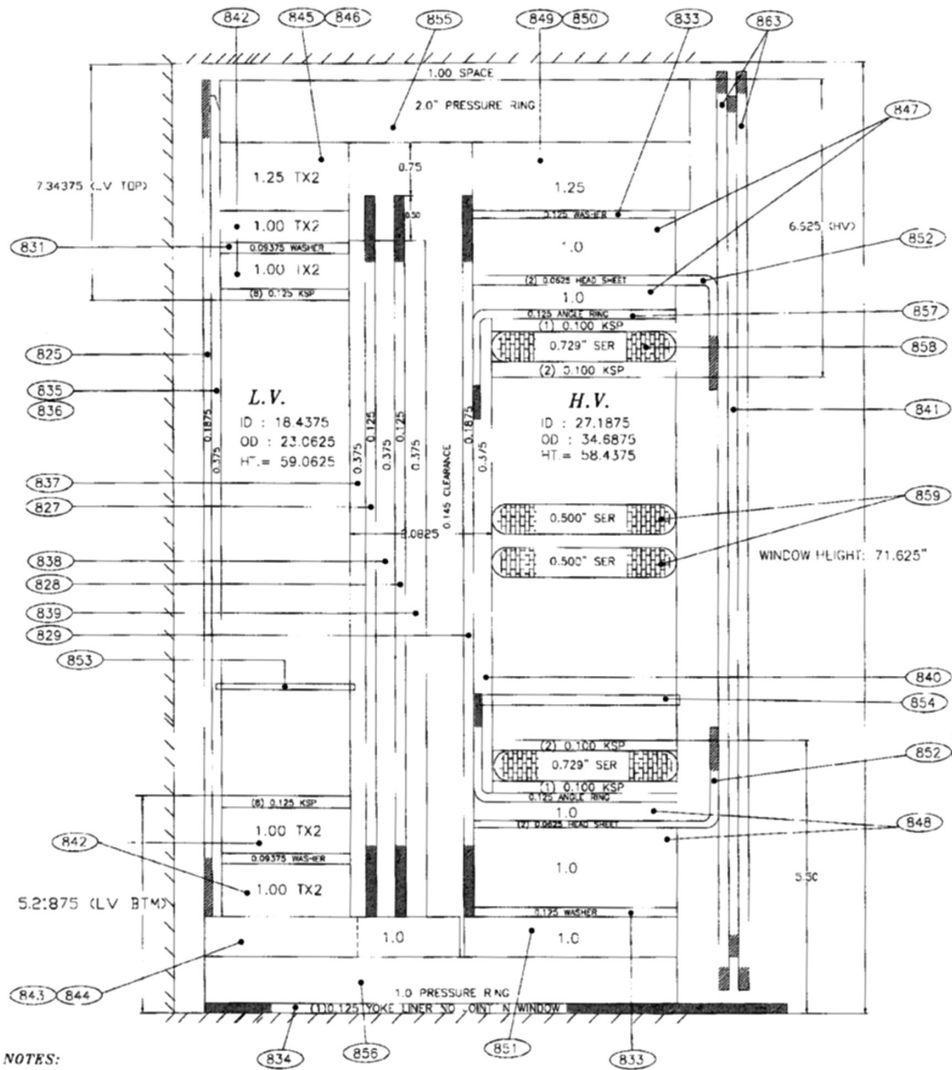
FIGURE 2.4
Core–coil–insulation coordination for a transformer.

2.2.20 Other Aspects

- Connection diagram: What are the standard connections of the PV application transformers?
- Shielding requirements (electrostatic shielding, protective shielding, harmonic filtration shielding).
- Inverter technology: Inverter technology has been slow to advance, because it is an electronic technology. It remains to be seen whether this comparative disadvantage will be a fatal flaw in the advancement of solar technology to the same level as wind farms in the renewable energy arena.

- Size of installation: The size of solar farms is limited by inverter technology, since inverters can currently only be built to about 500 kVA. This means that nearly all solar applications use pairs of 500 kVA inverters to drive the transformer and produce about 1000 kVA. Increasing the size by adding more inverters into one transformer box is extremely difficult, due to the complexities associated with the size of the box required and the practicalities of running cabling to convert from DC to AC.

Some of the core needs of DPV-GTs are

- Efficient heat management: The heat generated due to the uneven cooling of the coils leads to the creation of hot spots. This leads to the premature breakdown of the transformers.
- Lower harmonics and grid disturbances.
- The ability to withstand harsh weather conditions, temperatures, seismic levels and so on.

If necessary, DPV-GTs are designed and constructed to meet and exceed earthquake standards. Sometimes, DPV-GTs are rated for installation in the highest earthquake rating zones. In addition, it can incorporate a variety of fluids, including less flammable fluids required for enclosed applications.

DPV grid step-up transformers are especially designed to meet the solar industry's need for reliable service in remote locations and should offer advanced fault survivability/capability.

2.3 Relevant and Important Conclusions

DPV-GT solar converter step-up transformers are uniquely designed to connect solar farms to the electricity grid in large-scale solar power installations.

Step-up transformers are reliable and efficient engineered solutions with the necessary design flexibility needed for the solar industry. DPV-GTs are designed for the additional loading associated with the non-sinusoidal harmonic frequencies often found in inverter-driven transformers, and designs with multiple windings should be considered in case they can reduce transformer cost, minimize the transformer's footprint and provide the required functionality. Shell-type transformers can be also considered for this application.

The duty cycle seen in solar farms may not be as severe as those in wind farms, but solar power has its share of special considerations that affect transformer design. Those engaged in harnessing solar energy need to pay heed to these special needs to ensure that the solar installation is cost-effective and reliable.

References

1. Considerations for Power Transformers Applied in Distributed Photovoltaic (DPV): Grid Application, DPV-Grid Transformer Task Force Members, Power Transformers Subcommittee, IEEE-TC, Hemchandra M. Shertukde (chair), Mathieu Sauzay (vice chair), Aleksandr Levin (secretary), Enrique Betancourt, C. J. Kalra, Sanjib K. Som, Jane Verner, Subhash Tuli, Kiran Vedante, Steve Schroeder, Bill Chu, white paper in preparation for final presentation at the IEEE-TC conference in San Diego, CA, April 10–14, 2011.
2. C57.91: IEEE Guide for Loading Mineral-Oil-Immersed Transformers, 1995. Correction 1-2002.
3. Std. 519: Recommended Practices and Requirements for Harmonic Control in Electrical Power Systems, 1992.
4. C57.129: IEEE Standard for General Requirements and Test Code for Oil-Immersed HVDC Convertor Transformer, 1999 (2007 approved).
5. C57.18.10a: IEEE Standard Practices Requirements for Semiconductor Power Rectifier Transformers, 1998. Amended in 2008.
6. C57.110: IEEE Recommended Practice for Establishing Liquid-Filled and Dry-Type Power and Distribution Transformer Capability When Supplying Non-sinusoidal Load Current, 2008.
7. UL 1741: A Safety Standard for Distributed Generation, 2004.
8. Std. 1547.4: Draft Guide for Design, Operation and Integration of Distributed Resource Island Systems with Electric Power System, Only 1547.1 Is There, 2005.

3

Generalized Machine Theory and Reference Frame Formulation

3.1 Generalized Machine Theory and Reference Frame Formulation

Generalized machine theory (GMT) is developed on the hypothesis laid down by Park in 1926. This idea was then simplified by Kron and later further simplified by Gibbs using matrix algebra, to make the design and evaluation easily computable. The main consideration in this theory was to develop the equivalent circuit of rotating machines using the orthogonal direct and quadrature (*d-q*) axes as the basis vectors, as shown in Figure 3.1 for a salient two-pole synchronous machine.

The *d*-axis is in line with the magnetic north pole. θ is the angle between the *d*-axis and the reference axis. The *q*-axis is orthogonal to the *d*-axis. Generally, the three-phase equivalent circuits of rotating machines are developed using three-phase phasors of lines *a*, *b* and *c*, respectively. Thus, as shown in Chapter 2, we have the phasors for each phase as

$$V_{an}, V_{bn}, V_{cn} \tag{3.1}$$

where the second subscript of all variables in Equation 3.1 represents the neutral point of a four-wire system. The resulting line-to-line voltages would be

$$V_{ab}, V_{bc}, V_{ca} \tag{3.2}$$

Similarly, the phase currents and line-to-line currents are given by

$$I_{an}, I_{bn}, I_{cn} \tag{3.3}$$

$$I_{ab}, I_{bc}, I_{ca} \tag{3.4}$$

We now proceed to apply the theory of GMT to synchronous machines by conducting the *d-q* modeling as follows.

In addition to the *d-q* axes, we add one more axis, which is the reference zero axis colinear with the horizontal, such that it has a zero-phase shift. This converts the *d-q* axes to a *d-q*-0 transformation, as shown in Figure 3.2. It thus becomes a tensor that rotates the reference frame of a three-element vector or a similar 3×3 matrix in order to simplify the final analysis, as mentioned earlier. This *d-q*-0 transformation can be used in electrical engineering with a three-phase power system and applied to three-phase variables in Equations 3.1 through 3.4. The *d-q*-0 transform is used to rotate the reference frames of
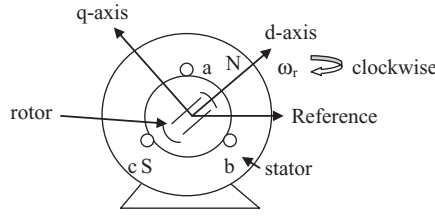
FIGURE 3.1
d-q axis of a salient two-pole synchronous machine.
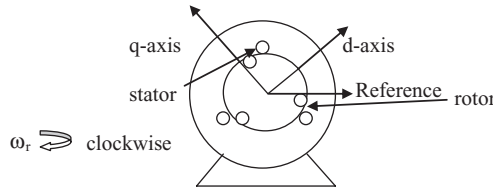
FIGURE 3.2
d-q-0 representation of polyphase IM.

the AC waveforms of variables in the above equations to align them such that the final alignment is necessarily visualized as DC transformation. Thus, if the analysis is applied to a three-phase synchronous machine, the *d-q*-0 transformation transforms the stator and rotor variables into a single-phase DC rotating frame to eliminate the effects of time-varying inductances. Another example is the use of the transform to calculate the control of three-phase inverters.

We will use subscripts *r* for rotor parameters and *s* for stator parameters and *q*, *d* and 0 for the corresponding *d-q*-0 transformations while relating with the *abc* three-phase parameters. Thus, for the stator it is

$$f_{qd0s} = K_s f_{abcs} \tag{3.5}$$

and for the rotor it is

$$f_{qd0r} = K_r f_{abcr} \tag{3.6}$$

where function *f* in Equations 3.5 and 3.6 represents any of the electrical parameters, as in Equation 3.7:

$$f = \text{voltage, current, flux linkage or charge} \tag{3.7}$$

and for a stator and a distributed rotor, respectively, as follows:

$$\left(f_{qd0s} \right)^T = \begin{bmatrix} f_{qs} & f_{ds} & f_{0s} \end{bmatrix} \tag{3.8}$$

$$\left(f_{qd0r} \right)^T = \begin{bmatrix} f_{qr} & f_{dr} & f_{0r} \end{bmatrix} \tag{3.9}$$

with the 3×3 transformation matrix K_s given by

$$K_s = \frac{2}{3}\begin{bmatrix} \cos\theta & \cos(\theta-120) & \cos(\theta+120) \\ \sin\theta & \sin(\theta-120) & \sin(\theta+120) \\ \dfrac{1}{2} & \dfrac{1}{2} & \dfrac{1}{2} \end{bmatrix} \tag{3.10}$$

and

$$(K_s)^{-1} = \begin{bmatrix} \cos\theta & \sin\theta & 1 \\ \cos(\theta-120) & \sin(\theta-120) & 1 \\ \cos(\theta+120) & \sin(\theta+120) & 1 \end{bmatrix} \tag{3.11}$$

with

$$\omega = \frac{d\theta}{dt} \tag{3.12}$$

The resulting three-phase electrical power in the stator of the synchronous machine is given by

$$P_{abcs} = V_{as}I_{as} + V_{bs}I_{bs} + V_{cs}I_{cs} \tag{3.13}$$

The resulting power in the *d-q-0* transformation is as follows:

$$P_{dq0s} = \frac{2}{3}\left[V_{ds}I_{ds} + V_{dq}I_{qs} + V_{0s}I_{0s}\right] = P_{abcs} \tag{3.14}$$

Using this transformation, stationary circuit variables can be easily transformed to the arbitrary reference base frame. We can now generate the variables for a resistive circuit, assuming the stator winding has a realistic resistance R_s, as follows:

$$V_{abcs} = R_s I_{abcs} \tag{3.15}$$

Using Equations 3.10, 3.11, 3.13 and 3.14, the voltage in the stator winding resistance is given by

$$V_{dq0s} = K_s R_s \left[K_s\right]^{-1} I_{dq0s} \tag{3.16}$$

For a three-phase stator, R_s is the resistance matrix.

When the machine is symmetrical or balanced in all phases, R_s is a diagonal matrix and its non-zero elements along the diagonal are equal, which results in

$$K_s R_s \left[K_s\right]^{-1} = R_s \tag{3.17}$$

When the machine phases are unequal or unbalanced (i.e., asymmetrical), phase resistances are unequal; therefore, the *d-q-0* variables contain sinusoidal functions of θ, except when ω = 0.

We can now develop the transformation for the inductive elements in the stator winding by evaluating the time derivative of the flux linkage, as follows:

$$V_{abcs} = \frac{d}{dt}\left(\lambda_{abcs}\right) \tag{3.18}$$

Thus, the transformed voltage in the *d-q*-0 axes is

$$V_{dq0s} = K_s\left\{\frac{d}{dt}[K_s]^{-1}\left(\lambda_{dq0s}\right)\right\} \tag{3.19}$$

$$V_{dq0s} = K_s\left\{\frac{d}{dt}[K_s]^{-1}\right\}\left(\lambda_{dq0s}\right) + K_s K_s^{-1}\frac{d}{dt}\left(\lambda_{dqos}\right) \tag{3.20}$$

where:

$$\left\{\frac{d}{dt}[K_s]^{-1}\right\} = \omega\begin{bmatrix} -\sin\theta & \cos\theta & 0 \\ -\sin(\theta-120) & \cos(\theta-120) & 0 \\ -\sin(\theta+120) & \cos(\theta+120) & 0 \end{bmatrix} \tag{3.21}$$

which yields

$$K_s\left\{\frac{d}{dt}[K_s]^{-1}\right\} = \omega\begin{bmatrix} 0 & 1 & 0 \\ -1 & 0 & 0 \\ 0 & 0 & 0 \end{bmatrix} \tag{3.22}$$

Using Equation 3.22 in Equation 3.20 yields

$$V_{dq0s} = \omega\left(\lambda_{dq0s}\right) + \frac{d}{dt}\left(\lambda_{dqos}\right), \text{ where } \omega = \frac{d\theta}{dt} \tag{3.23}$$

which can be expanded as

$$V_{qs} = \omega\lambda_{ds} + \frac{d}{dt}\lambda_{qs} \tag{3.24}$$

$$V_{ds} = -\omega\lambda_{qs} + \frac{d}{dt}\lambda_{ds} \tag{3.25}$$

and

$$V_{0s} = \frac{d}{dt}\lambda_{0s} \tag{3.26}$$

All the preceding equations can be tabulated for several conditions, as follows.

1. Arbitrary reference frame

   In the arbitrary reference frame, the reference frame speed is ω and is generally not specified. The interpretation is related to stationary circuit variables referred to the stationary arbitrary reference frame. The variables involved are given by

$$\left(f_{dq0s}\right)^T = \begin{bmatrix} f_{ds} & f_{qs} & f_{0s} \end{bmatrix}, \text{ and } K_s \tag{3.27}$$

2. Stationary reference frame

In the stationary reference frame, the reference frame speed is zero and the stationary circuit variables referred to the stationary reference frame are specified as

$$\left(f^s{}_{dq0s}\right)^T = \begin{bmatrix} f^s{}_{ds} & f^s{}_{qs} & f_{0s} \end{bmatrix}, \text{ and } K^s{}_s \tag{3.28}$$

3. Rotor reference frame

In the rotor reference frame, the reference speed is ω_r and the stationary circuit variables referred to the reference frame are given by

$$\left(f^r{}_{dq0s}\right)^T = \begin{bmatrix} f^r{}_{ds} & f^r{}_{qs} & f_{0s} \end{bmatrix}, \text{ and } K^r{}_s \tag{3.29}$$

4. Synchronously rotating reference frame

In the synchronously rotating reference frame, the reference frame speed is ω_e and the variables referred to the reference frame are given by

$$\left(f^e{}_{dq0s}\right)^T = \begin{bmatrix} f^e{}_{ds} & f^e{}_{qs} & f_{0s} \end{bmatrix}, \text{ and } K^e{}_s \tag{3.30}$$

In the preceding reference frames, the *s* subscript denotes variables and transformations associated with circuits that are stationary, as in a stator for an electrical machine, as opposed to the *r* subscript, which refers to rotor circuits, which generally rotate. The superscripts are related to *ds* and *qs* variables and transformations associated with a specific reference frame, as in the ones described previously, except in the arbitrary reference frame that carries no superscript index. This is because the 0*s* variables are independent of ω and thus not associated with a reference frame, and thus no superscript is assigned to f_{0s}. The transformation of variables associated with stationary circuits to a stationary reference frame was developed by E. Clarke, who used the notations

$$\begin{bmatrix} f_\alpha & f_\beta & f_0 \end{bmatrix} \text{ instead of } \begin{bmatrix} f^s{}_{ds} & f^s{}_{qs} & f_{0s} \end{bmatrix} \tag{3.31}$$

In Park's transformations to the rotor reference, he used

$$\begin{bmatrix} f_d & f_q & f_0 \end{bmatrix} \text{ instead of } \begin{bmatrix} f^r{}_{ds} & f^r{}_{qs} & f_{0s} \end{bmatrix} \tag{3.32}$$

which indicates no established notation for the variables in the synchronously rotating reference frame. The voltage equation for all reference frames can be obtained from those in the arbitrary reference frame. The transformations for a specific reference frame are obtained by substituting the appropriate reference frame speed for ω. In most cases, the initial or time-zero displacements can be selected equal to zero. However, there are situations where the initial displacement of the reference frame to which the variables are being transformed will not generally be zero.

In some derivations and further analysis, it is convenient to relate the variables of one reference to the variables of another reference frame directly, without involving the *abc* variables in the transformation. This can be achieved as follows.

Let *i* be the reference frame from which the variables are being transformed and *j* be the reference frame to which the variables are being transformed; then

$$f^{j}{}_{dq0s} = {}^{i}K^{j}f^{i}{}_{dq0s} \tag{3.33}$$

$$f^{i}{}_{dq0s} = K^{i}{}_{s}f_{abcs} \tag{3.34a}$$

Thus,

$$f^{j}{}_{dq0s} = {}^{i}K^{j}K^{i}{}_{s}f_{abcs} \tag{3.34b}$$

and

$$f^{j}{}_{dq0s} = K_{s}{}^{j}f_{abcs} \tag{3.35}$$

which yields

$${}^{i}K^{j}K^{i}{}_{s} = K_{s}{}^{j} \tag{3.36}$$

Thus,

$${}^{i}K^{j} = K_{s}{}^{j}(K_{s}{}^{i})^{-1} \tag{3.37}$$

and thus,

$${}^{i}K^{j} = \begin{bmatrix} \cos(\theta_{j} - \theta_{x}) & -\sin(\theta_{j} - \theta_{x}) & 0 \\ \sin(\theta_{j} - \theta_{x}) & \cos(\theta_{j} - \theta_{x}) & 0 \\ 0 & 0 & 1 \end{bmatrix} \tag{3.38}$$

We now proceed to apply this to generalized machines in electrical engineering.

3.2 Generalized Machine Model

All electrical machines can be represented by a generalized model, as proposed by Krone, and is basically a hypothetical machine. This idea is based on some assumptions, as follows:

1. As the distribution of the current along the air gap periphery and flux is repetitive in nature after every pole pair, a generalized machine is assumed to have one pole pair in order to avoid complicacy and to avoid the conversion of the electrical and mechanical angles.
2. For simplification, every generalized machine has a single coil.
3. As shown in Figure 3.1, the *d*-axis is co-linear with the magnetic axis (N–S pole). The *q*-axis is orthogonal to the *d*-axis.
4. The direction of the current and flux is governed by the right-hand thumb (RHT) rule. If the current is in the direction of the RHT, then the magnetic flux is in the direction of all other fingers curled around the direction of the thumb.

5. *V* and *I* represent the voltage externally impressed on the coil and the current, the magnitude and the direction of the current flowing in the coil. See assumption 4.

6. The machine is assumed to be rotating in the positive direction when rotating in the clockwise direction.

7. Subscripts *s*, *r*, *d* and *q* are used for stator, rotor, direct-axis and quadrature-axis, respectively.

Using the preceding assumptions, the voltage equations of the generalized machine shown in Figure 4.1 can be written as follows:

$$V_{ds} = \left(R_{ds} + L_{ds}\frac{d}{dt} \right) I_{ds} + M_d \frac{d}{dt} I_{dr} \tag{3.39}$$

$$V_{qs} = \left(R_{qs} + L_{qs}\frac{d}{dt} \right) I_{qs} + M_q \frac{d}{dt} I_{qr} \tag{3.40}$$

$$V_{dr} = M_d \frac{d}{dt} I_{ds} - M_q \omega_r I_{qs} + \left(R_{dr} + L_{dr}\frac{d}{dt} \right) I_{dr} - \omega_r L_{qr} I_{qr} \tag{3.41}$$

$$V_{qr} = M_d \omega_r \frac{d}{dt} I_{ds} + M_q \frac{d}{dt} I_{qs} + \left(R_{qr} + L_{qr}\frac{d}{dt} \right) I_{qr} + \omega_r L_{dr} I_{dr} \tag{3.42}$$

where:

$$V_{ds}, V_{qs}, V_{dr}, V_{qr} \text{ are direct-axis and quadrature-axis voltages} \tag{3.43}$$

In a practical machine, these voltages can be transformed from the *abc* variables by using Equations 3.5 through 3.12.

$$I_{ds}, I_{qs}, I_{dr}, I_{qr} \text{ are direct-axis and quadrature-axis currents} \tag{3.44}$$

In a practical machine these currents can be transformed from the *abc* variables by using Equations 3.5 through 3.12.

$$r_{ds}, r_{qs}, r_{dr}, r_{qr} \text{ are direct-axis and quadrature-axis resistances} \tag{3.45}$$

$$L_{ds}, L_{qs}, L_{dr}, L_{qr} \text{ are direct-axis and quadrature-axis self-inductances} \tag{3.46}$$

$$M_d, M_q \text{ are direct-axis and quadrature-axis mutual inductances} \tag{3.47}$$

The values of all the preceding parameters depend on the machine and the shape of the rotor: that is, salient or distributed in structure. Besides, all these parameters are assumed to be linear, time invariant and causal to be suitable for system analysis using generalized machine theory. This leads to a matrix-form representation, as follows:

$$
\begin{vmatrix} V_{ds} \\ V_{qs} \\ V_{dr} \\ V_{qr} \end{vmatrix} = \begin{bmatrix} R_{ds} + L_{ds}\dfrac{d}{dt} & 0 & M_d\dfrac{d}{dt} & 0 \\ 0 & R_{qs} + L_{qs}\dfrac{d}{dt} & 0 & M_q\dfrac{d}{dt} \\ M_d\dfrac{d}{dt} & -M_q\omega_r & R_{dr} + L_{dr}\dfrac{d}{dt} & -\omega_r L_{qr} \\ M_d\omega_r & M_q\dfrac{d}{dt} & \omega_r L_{dr} & R_{qr} + L_{qr}\dfrac{d}{dt} \end{bmatrix} \begin{vmatrix} I_{ds} \\ I_{qs} \\ I_{dr} \\ I_{qr} \end{vmatrix} \tag{3.48}
$$

which can be written in matrix form as $[V] = [Z][I]$,
where:

$$
[Z] = \begin{bmatrix} R_{ds} + L_{ds}\dfrac{d}{dt} & 0 & M_d\dfrac{d}{dt} & 0 \\ 0 & R_{qs} + L_{qs}\dfrac{d}{dt} & 0 & M_q\dfrac{d}{dt} \\ M_d\dfrac{d}{dt} & -M_q\omega_r & R_{dr} + L_{dr}\dfrac{d}{dt} & -\omega_r L_{qr} \\ M_d\omega_r & M_q\dfrac{d}{dt} & \omega_r L_{dr} & R_{qr} + L_{qr}\dfrac{d}{dt} \end{bmatrix} \tag{3.50}
$$

That is,

$$
[Z] = [R] + [L]\frac{d}{dt} + [G]\omega_r
$$

where the resistance matrix is

$$
[R] = \begin{bmatrix} R_{ds} & 0 & 0 & 0 \\ 0 & R_{qs} & 0 & 0 \\ 0 & 0 & R_{dr} & 0 \\ 0 & 0 & 0 & R_{qr} \end{bmatrix} \tag{3.51}
$$

The self-inductance matrix is

$$
[L] = \begin{bmatrix} L_{ds} & 0 & M_d & 0 \\ 0 & L_{qs} & 0 & M_q \\ M_d & 0 & L_{dr} & 0 \\ 0 & M_q & 0 & L_{qr} \end{bmatrix} \tag{3.52}
$$

and the speed-dependent component is

$$
[G] = \begin{bmatrix} 0 & 0 & 0 & 0 \\ 0 & 0 & 0 & 0 \\ 0 & -M_q & 0 & -L_{qr} \\ 0 & 0 & L_{dr} & 0 \end{bmatrix} \tag{3.53}
$$

We can now evaluate the real power, imaginary power and rotational power as part of the total power equation as follows:

$$P = [I]^T [V] = V_{ds}I_{ds} + V_{qs}I_{qs} + V_{dr}I_{dr} + V_{qr}I_{qr}$$

$$= \left[I \right]^T [R][I] + \left[I \right]^T [L]\frac{d}{dt}[I] + \omega_r[I]^T [G][I] \tag{3.54}$$

where the copper loss is

$$P_{cu} = [I]^T [R][I] = I^2_{ds}R_{ds} + I^2_{qs}R_{qs} + I^2_{dr}R_{dr} + I^2_{qr}R_{qr} \tag{3.55}$$

the change in stored energy is

$$P_{se} = [I]^T [L]\frac{d}{dt}[I] \tag{3.56}$$

and the electrical power converted to mechanical power is

$$P_{rot} = \omega_r[I]^T [G][I] \tag{3.56}$$

resulting in the electrical torque, developed as

$$\tau_e = \frac{P_{rot}}{\omega_r} = [I]^T [G][I] \tag{3.57}$$

$$= I_{qr}M_dI_{ds} - M_qI_{dr}I_{qs} + \left(L_{dr} - L_{qr}\right)I_{qr}I_{dr} \tag{3.58}$$

In Equation 3.58, when the term $(L_{dr} - L_{qr})$ is zero, the third term goes to zero and is related to the reluctance torque, which is zero in the absence of salient poles and is achieved in distributed pole conditions. As we know, the difference between electrical torque and load torque generates the dynamics of the machine, as follows:

$$\tau_e - \tau_L = J\dot{\omega}_r \tag{3.59}$$

3.3 *d-q*-0 Analysis of Three-Phase Induction Motor

We consider here a polyphase induction machine (IM), which necessitates that the *d-q*-0 axes be fixed in the stator structure as shown in Figure 3.2.

The stator is shown offset from the rotor to highlight the slip action. The variable θ is the angle between the d-axis and the reference axis. As the three-phase stator windings are stationary (*a-b-c*) along with the *d-q*-0 axes with respect to each other, the transformation matrix from (*a-b-c*) to (*d-q*-0) or vice a versa has constant coefficients. The transformation matrix is shown as

$$\begin{bmatrix} I_{ds} \\ I_{qs} \\ I_{0s} \end{bmatrix} = \frac{2}{3} \begin{bmatrix} \cos\theta & \cos(\theta-120) & \cos(\theta+120) \\ \sin\theta & \sin(\theta-120) & \sin(\theta+120) \\ \frac{1}{2} & \frac{1}{2} & \frac{1}{2} \end{bmatrix} \begin{bmatrix} I_a \\ I_b \\ I_c \end{bmatrix} \tag{3.60}$$

and

$$
\begin{bmatrix} V_{ds} \\ V_{qs} \\ V_{0s} \end{bmatrix} = \frac{2}{3} \begin{bmatrix} \cos\theta & \cos(\theta-120) & \cos(\theta+120) \\ \sin\theta & \sin(\theta-120) & \sin(\theta+120) \\ \dfrac{1}{2} & \dfrac{1}{2} & \dfrac{1}{2} \end{bmatrix} \begin{bmatrix} V_a \\ V_b \\ V_c \end{bmatrix}
\tag{3.61}
$$

In Equations 3.60 and 3.61, the subscript *s* stands for the stator; the *d-q*-0 currents and voltages are with respect to the stator. Note that in reality the rotor is short-circuited on itself in an IM. The three-phase currents in the stator in the time domain are given by

$$
I_A = I_m \cos(\omega t + \alpha)
\tag{3.62}
$$

$$
I_B = I_m \cos(\omega t + \alpha + 120)
\tag{3.63a}
$$

$$
I_C = I_m \cos(\omega t + \alpha - 120)
\tag{3.63b}
$$

where:
Peak value I_m is the $\sqrt{2}$ times the RMS value of the current
α is the phase angle of the respective phase current in the time domain origin
Thus, from Equations 3.60 and 3.61 we have

$$
\begin{bmatrix} I_{ds} \\ I_{qs} \end{bmatrix} = \sqrt{\frac{2}{3}} \begin{bmatrix} I_m \cos(\omega t + \alpha) \\ I_m \sin(\omega t + \alpha) \end{bmatrix}
\tag{3.64}
$$

and

$$
\begin{bmatrix} V_{ds} \\ VI_{qs} \end{bmatrix} = \sqrt{\frac{2}{3}} \begin{bmatrix} V_m \cos(\omega t + \alpha) \\ V_m \sin(\omega t + \alpha) \end{bmatrix}
\tag{3.64}
$$

From Equations 3.63 and 3.64 it is clear that the *d-q* axes currents as well as voltages are functions of time and are displaced by 90°, which shows that *d-q* currents constitute a two-phase system of currents having a frequency of the equivalent three-phase system. While this analysis is for a distributed rotor system of winding connections in a squirrel cage IM, the rotor is short-circuited on itself, which causes the voltages V_{dr} and V_{qr} to go to zero, resulting in the reversal of currents I_{dr} and I_{qr}, as shown in Equation 3.65:

$$
\begin{vmatrix} V_{ds} \\ V_{qs} \\ 0 \\ 0 \end{vmatrix} = \begin{bmatrix} R_{ds} + L_{ds}\dfrac{d}{dt} & 0 & -M_d\dfrac{d}{dt} & 0 \\ 0 & R_{qs} + L_{qs}\dfrac{d}{dt} & 0 & -M_q\dfrac{d}{dt} \\ M_d\dfrac{d}{dt} & -M_q\omega_r & -\left(R_{dr} + L_{dr}\dfrac{d}{dt}\right) & \omega_r L_{qr} \\ M_d\omega_r & M_q\dfrac{d}{dt} & -\omega_r L_{dr} & -\left(R_{qr} + L_{qr}\dfrac{d}{dt}\right) \end{bmatrix} \begin{vmatrix} I_{ds} \\ I_{qs} \\ I_{dr} \\ I_{qs} \end{vmatrix}
\tag{3.65}
$$

Thus, from all the analysis shown in the previous sections it is understood that the GMT approach to synchronous machines and IMs is simpler than the coupled circuit approach, as long as matrix algebra is appropriately understood and applied. GMT makes use of simple concepts of electric circuits and provides a link between the three-phase system variables (*a-b-c*) and two-phase system variables (*d-q*). For further simplicity, a reference zero axis is added to obtain matrix algebra convenience in the manipulations of the *d-q*-0 axes system.

Problems

PROBLEM P.3.1

Under steady-state operating conditions, the armature of the salient-pole synchronous generator carries symmetrical sinusoidal three-phase currents.

$$i_a = \sqrt{2}\,|I_a|\sin\left(\theta_d - \theta_a\right)$$

$$i_b = \sqrt{2}\,|I_a|\sin\left(\theta_d - 120° - \theta_a\right)$$

$$i_c = \sqrt{2}\,|I_a|\sin\left(\theta_d - 240° - \theta_a\right)$$

where:

$$\theta_d = \omega t + \delta + 90°$$

Using the P-transformation matrix, find expressions for the corresponding *d-q*-0 currents of the armature.

PROBLEM P.3.2

DC current I_f is supplied to the filed winding of an unloaded salient-pole synchronous generator rotating with constant angular velocity ω. Find the form of the *oc* armature voltages and their *d-q*-0 components.

PROBLEM P.3.3

The armature of a three-phase salient pole generator carries the currents

$$i_a = \sqrt{2}\,|1000|\sin\left(\theta_d - \theta_a\right)A$$

$$i_b = \sqrt{2}\,|1000|\sin\left(\theta_d - 120° - \theta_a\right)A$$

$$i_c = \sqrt{2}\,|1000|\sin\left(\theta_d - 240° - \theta_a\right)A$$

1. Using the P-transformation matrix, find the direct axis current i_d and the quadrature axis current i_q.
2. What is the zero-sequence current i_0?
3. Suppose the armature currents are

$$i_a = \sqrt{2}\,|1000|\sin\left(\theta_d - \theta_a\right) A$$

$$i_b = i_c = 0$$

Find i_d, i_q and i_0.

4

Transmission Lines

4.1 Parameters

The three parameters of a transmission line that define its equivalent circuit are

1. Resistance
2. Inductance
3. Capacitance

There are several passive components in a single-line diagram (SLD) that are associated with many of the major components of a power system. One of the most important components is the resistance. The resistance of any electrical conductor is given by

$$R = \rho \frac{l}{A} \, \Omega \tag{4.1}$$

where:
  ρ is the resistivity of the material of the conductor
  l is its length in meters
  A is the area of the cross-section of the material

The resistivities of different materials are listed in Table 4.1.

The DC resistance of stranded conductors as calculated by Equation 4.1 is greater than its effective value, described in Equation 4.2:

$$R = \frac{P}{\left| I^2 \right|} \, \Omega \tag{4.2}$$

where:
  P is the power loss in the conductor
  I is the current in the conductor

This effective DC resistance is different in stranded conductors due to the spiraling of the conductors. Spiraling causes some of the strands to be longer than the central core conductor. This increase is approximately 1% more for three-strand conductors and 2% for concentrically stranded conductors. In addition, the AC resistance of conductors is different due to the *skin effect*. With different frequencies of current flowing in the conductor, the current tends to flow more in the area of cross-section closer to the skin of the conductor.

TABLE 4.1

Material	ρ ($\Omega \cdot$m) at 20°C
Hard-drawn copper	1.77×10^{-8}
Aluminum	2.83×10^{-8}

Thus, the area of cross-section to be used in the denominator of Equation 4.1 is reduced, leading to an increase in the ohmic value. Besides, the resistance of metallic conductors varies with temperature, as shown in Figure 4.1. Temperature t is plotted on the vertical axis in degrees Celsius and resistance R on the horizontal axis in ohms. R_1 and R_2 are the resistances at temperatures t_1 and t_2, respectively. The extended line cuts the vertical axis, generating the value T. This value T is tabulated in Table 4.2 for different kinds of conductors and different materials.

$$\frac{R_2}{R_1} = \frac{T + t_2}{T + t_1} \tag{4.3}$$

or

$$R_2 = R_1 \left[1 + \alpha \left(T_2 - T_1 \right) \right] \tag{4.4}$$

where α is the temperature coefficient of resistance.

The resistivity of a material as given in Equation 4.1 is related to the conductivity σ of the material, as shown in Equation 4.5:
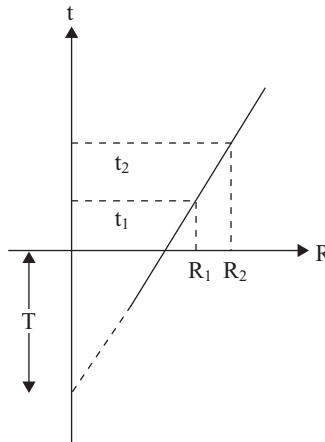
FIGURE 4.1
Variation of resistance of metallic conductors with temperature.

TABLE 4.2

Material	T
Annealed copper of 100% conductivity	234.5
Hard-drawn copper of 97.3% conductivity	241
Hard-drawn aluminum of 61% conductivity	228

TABLE 4.3

Material	Conductivity σ (S/m)	Resistivity ρ at 20°C (μΩ·cm)
Annealed copper of 100% conductivity	5.96×10^7	1.72
Hard-drawn copper of 97.3% conductivity	5.80×10^7	1.77
Hard-drawn aluminum of 61% conductivity	3.50×10^7	2.83

$$\sigma = \frac{1}{\rho} \qquad (4.5)$$

This is shown in Table 4.3 for different materials.

The unit of conductivity is Siemens per meter, where Siemens (after the famous German scientist) is written as *mhos* (*mho* is the inverse of *ohm*).

4.2 Inductance *L* in Henry

The next important passive element that comprises a common and essential part of the SLD is the inductance *L* of a single-conductor coil, measured in units of henry (H). This is used to represent all components, including transmission lines, transformers and rotating machines both AC as well as DC. In general, inductance is given by Equation 4.6:

$$L = N^2 \wp = N^2 / \mathcal{R} \qquad (4.6)$$

where:
  N is the number of turns of the coil
  $\wp$ is the permeance, which is the inverse of $\mathcal{R}$, as given in Equations 4.7 and 4.8, respectively:

$$\wp = \frac{1}{\mathcal{R}} \qquad (4.7)$$

$$\mathcal{R} = \frac{l}{\mu A} \qquad (4.8)$$

where:
  μ is the permeability of the magnetic medium
  l is the length of the magnetic circuit in meters (m)
  A is the area of cross-section in square meters (m²)

In general, the inductance is evaluated by using Equation 4.9 for the constant permeability of the medium.

$$\lambda = N\Phi = LI \qquad (4.9)$$

where:
  Φ   is the magnetic flux permeating in the magnetic circuit
  λ = *N*Φ is the flux linkage
  I   is the current in amperes carried by the coil with inductance *L*

Equation 4.5 can be derived from Equation 4.8 as follows:

$$LI = NBA = N\mu HA = \frac{N\mu NIA}{l}$$

$$L = \frac{N^2}{\mathcal{R}} = N^2\wp, \text{ as in Equations 4.6 and 4.7}$$

where:

B is the magnetic flux density in tesla

H is the magnetic field intensity in ampere-turns/meter

B and H are related by Equation 4.10:

$$B = \mu H \tag{4.10}$$

μ is the permeability of the magnetic medium and is given by Equation 4.11 in terms of the absolute permeability of the air or free space, as follows:

$$\mu = \mu_r \mu_0 \tag{4.11}$$

where:

μ_r is the relative permeability of the magnetic medium

μ_0 is the permeability of space or air given by $4\pi \times 10^{-7}$ H/m

The relative permeabilities of different media are given in Table 4.4.

Thus, if one has more than one conductor—that is, several strands of conductors, as in aluminum conductor steel-reinforced (ACSR) cable—then it is easy to find the flux linkage of the total magnetic circuit and divide this product by the current I to yield the inductance L.

To find the inductance of a transmission line, further care must be taken to account for the following:

1. Internal flux of the conductor
2. External flux associated with the conductor

This necessitates the use of Faraday's law:

$$e = \frac{d}{dt}(N\Phi) \tag{4.12}$$

TABLE 4.4

Material	Relative Permeability
Air	1
Silicon steel	6,000–8,000
Super-magnetic Mu material	75,000–100,000
Nickel	250
Cobalt	600

and Equation 4.9:

$$e = L\frac{di}{dt} \tag{4.13}$$

which yields

$$L = \frac{d(N\Phi)}{di} \tag{4.14}$$

Thus,

$$\Psi = LI \text{ Wb·turn} \tag{4.15}$$

Once the current changes to AC, both the internal and external flux linkages are also sinusoidal and results in a phasor, as follows:

$$\Psi = LI \text{ Wb·turn} \tag{4.16}$$

Ψ and I are in phase, and L results in a phasor voltage drop, as follows:

$$V = j\omega LI \text{ volts} \tag{4.17}$$

$$V = j\omega\Psi \text{ volts} \tag{4.18}$$

Besides the preceding kinds of fluxes, there is one more called the *mutual flux*, which results in the *mutual inductance*. This helps to analyze the influence of power lines on telephone lines as well as coupling between parallel lines. Mutual inductance is evaluated by finding the flux linkages of one circuit due to the current in the second circuit in the proximity or in the near or far field per ampere of current in the second circuit. Thus,

$$M_{12} = \frac{\Psi_{12}}{I_2}\text{H} \tag{4.19}$$

where Ψ_{12} is the mutual flux linkage, as described previously between the two circuits interacting magnetically with each other.

Then, the corresponding voltage in the first circuit is

$$V_1 = j\omega M_{12}I_2 = j\omega\Psi_{12} \text{ volts} \tag{4.20}$$

4.2.1 Inductance of a Conductor Due to Internal Flux

Let us now proceed to find the inductance of a conductor due to internal flux. Changing the lines of flux inside the conductors contributes to the induced voltage of the electrical circuit. This flux links only a fraction of the total current flowing through the conductor of the transmission line under consideration, as shown in Figure 4.2.

A conductor with radius r carries a current I out of the page. The flux caused by this current moves counterclockwise (CCW), as shown in Figure 4.2. This flux links only with a fraction of the total current I. The return path of the current I in the conductor is far away, so that the lines of flux are concentric around and inside the conductor and CCW with
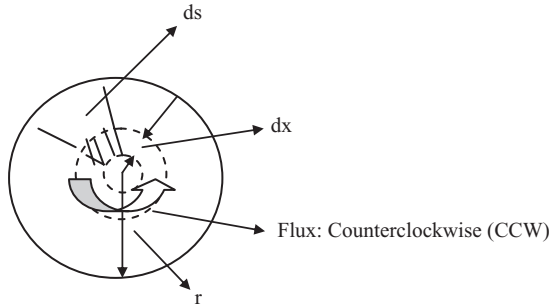
FIGURE 4.2
Conductor carrying current *I* out of the page; magnetic flux is CCW.

respect to the conductor. Using Ampere's integral law to calculate the magneto motive force (MMF) due to current *I* in the conductor, we have

$$MMF : I = \int J.da = \oint H.ds \ \ Wb.turn \tag{4.21}$$

where:
- *H*   is the magnetic field intensity tangential to *ds* in At/m
- *S*   is the distance along path, in meters
- *I*   is the current *A* that is enclosed in the circuit
- *J*   is the current density
- *A*   is the area through which current density *J* exists along the path of the current.

To analyze this further, let H_x be the magnetic field intensity at a distance *x* from the center of the conductor and H_x is constant at all points equidistant from the center. Using Equation 4.21, we have the current at distance *x* as

$$\oint H_x ds = I_x \tag{4.22}$$

Conducting the closed-loop integral over the path at a distance *x* from the center yields

$$2\pi x H_x = I_x \tag{4.23}$$

For an uniform current density *J* in the conductor, we have

$$I_x = \frac{\pi x^2}{\pi r^2} I \tag{4.24}$$

where *I* is the total current in the conductor.
Then,

$$H_x = \frac{I_x}{2\pi x}$$

$$= \frac{\pi x^2 I}{\pi r^2 \cdot 2\pi x}$$

$$= \frac{x \cdot I}{2\pi r^2} \ \ At/m \tag{4.25}$$

The magnetic flux density x m from the center of the conductor is

$$B_x = \mu H_x = \mu \frac{x.I}{2\pi r^2} \quad \frac{\text{Wb}}{\text{m}^2}$$ (4.26)

Therefore, the flux per meter of the length of the conductor is

$$d\Phi = \frac{\mu x I}{2\pi r^2} dx \quad \frac{\text{Wb}}{\text{m}^2}$$ (4.27)

where the area of the cross-section of the conductor associated with this incremental magnetic flux at distance x from the center of the conductor is

$$A = dx. \text{ axial length of the conductor}$$ (4.28)

yielding the flux linkage per meter of length of the conductor.

The linking fraction of the conductor turn of a radial element of thickness dx as a cylindrical element is as follows:

$$d\psi = \frac{\pi x^2}{\pi r^2} d\phi = \frac{\mu I x^3}{2\pi r^4} dx \text{ Wb.} \frac{\text{turn}}{\text{m}}$$ (4.29)

This results in the total flux linkage of a conductor due to internal flux, as follows:

$$\psi_{\text{int}} = \int_0^r \frac{\mu I x^3}{2\pi r^4} dx = \frac{\mu I}{8\pi}$$ (4.30)

For $\mu_r = 1$ and $\mu_0 = 4\pi \times 10^{-7}$ H/m:

$$\psi_{\text{int}} = \frac{I}{2} \times 10^{-7} \quad \text{Wb} - \frac{\text{turn}}{\text{m}}$$

which yields the inductance due to internal flux:

$$L_{\text{int}} = \frac{1}{2} \cdot 10^{-7} \quad \frac{\text{H}}{\text{m}}$$ (4.31)

We now proceed to find the inductance due to the external flux linkages caused by a current in a conductor. We start by assessing the flux linkages between two points external to an isolated current-carrying conductor. This is shown in Figure 4.3.

A circular conductor with radius r carries a current I out of the paper, as shown in Figure 4.3. According to Lenz's law, this creates a CCW magnetic flux, as shown within the radially thick dx concentric cylindrical tube along the length of the conductor assumed to be l m long. In this case as well, the return path is a far distance for mathematical analysis to conduct the overall MMF, as follows. For this analysis, two concentric circles at distances of D_1 and D_2 are shown in bold, where points P_1 and P_2 are shown and located. Dashed concentric circles are shown at a distance of x and $x + dx$ from the center of the conductor.
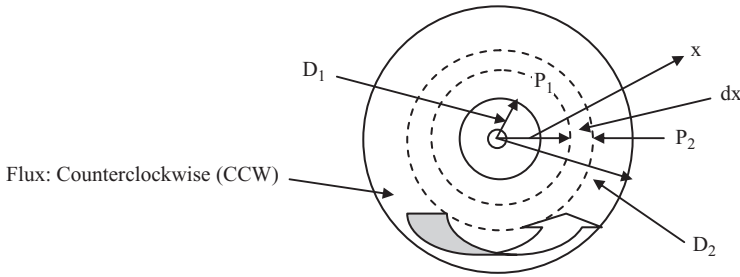
FIGURE 4.3
Single isolated conductor of radius *r* carrying current *I* out of the page and flux distribution around.

Thus, the total MMF at a distance x from the center of the conductor is given by

$$2\pi x H_x = I \tag{4.32}$$

where H_x is the magnetic field intensity at a distance x from the center of the conductor. This yields the magnetic flux density B_x, given by

$$B_x = \frac{\mu I}{2\pi x} \quad \frac{\text{Wb}}{\text{m}^2} \tag{4.33}$$

Therefore, the flux per meter of the length in the tubular element of thickness dx is given by

$$d\Phi = \frac{\mu I}{2\pi x} dx \quad \frac{\text{Wb}}{\text{m}} \tag{4.34}$$

where the area A through which the magnetic flux permeates is given by

$$A = dx \, x \, l \tag{4.35}$$

where l is the axial length of the conductor.

In the evaluation of the external flux linkage scenario it is imperative to observe that the flux linkages per meter are equal to the flux since all the flux external to the conductor links with all the current once (i.e., assuming there is only one single conductor accounting for the one single turn of the entire circuit) and the incremental flux linkage is now considered between the two points P_1 at distance D_1 and P_2 at distance D_2, respectively, from the center of the conductor due to current I in the conductor.

Thus,

$$\Psi_{12} = \int_{D_1}^{D_2} d\Psi = \int_{D_1}^{D_2} \frac{\mu I}{2\pi x} dx = \frac{\mu I}{2\pi} \ln \frac{D_2}{D_1} \quad \text{Wb} \cdot \frac{\text{turn}}{\text{m}} \tag{4.36}$$

Here, the permeability $\mu = \mu_r \mu_0$, where μ_r is the relative permeability of the medium in which the current carrying current I exists and μ_0 is the permeability of space given by $4\pi \times 10^{-7}$ H/m. Assuming $\mu_r = 1$, the mutual flux linkage is given as

$$\Psi_{12} = 2 \cdot 10^{-7} I \ln \frac{D_2}{D_1} \quad \text{Wb} \cdot \frac{\text{turn}}{\text{m}} \tag{4.37}$$

Thus the inductance only due to the flux included between the two points P_1 at distance D_1 and P_2 at distance D_2 respectively, is given by dividing Equation 4.37 by the current I carried by the conductor with radius r, as follows:

$$L_{12} = 2 \cdot 10^{-7} \ln \frac{D_2}{D_1} \quad \frac{H}{m}$$ (4.38)

We now extend this thought process to the following discussion to evaluate the *inductance of a single-phase two-wire transmission line*.

Figure 4.4 shows the two wires of the single-phase transmission line. Conductor *1* with radius r_1 carries current I out of the paper, resulting in a CCW magnetic flux. Conductor 2 with radius r_2 is the return circuit for the first conductor such that it carries a current into the paper. The back of the arrow $\otimes$ indicates the current entering the paper. For conductor 1, $\bigcirc$ indicates the direction of current coming out of the paper. In Figure 4.4, the dashed flux lines created by conductor 1 although are shown elliptically due to the paucity of space; these flux lines are actually concentric. The two conductors are separated by distance $D \gg r_1, r_2$.

One can now observe that

1. One conductor is the return circuit for the other. Thus, if conductor 1 carries a current of I, the second conductor 2 carries a current of $-I$.

2. A line of flux set up by the current in conductor 1 at a distance equal to or greater than $D + r_2$ from center of conductor 1 does not link the circuit and so cannot induce a voltage (using condition as in observation 1 above).

3. The fraction of the total current linked by a line of flux external to conductor 1 at a distance equal to or less than $D - r_2$ to $D + r_2$ the fraction changes from one to zero.

4. $D \gg r_1, r_2$.

Assuming that the external flux set up by the current in conductor 1 extending to the center of conductor 2 links all the current I and beyond the center of conductor 2 links none, as shown in Figure 4.4, this yields

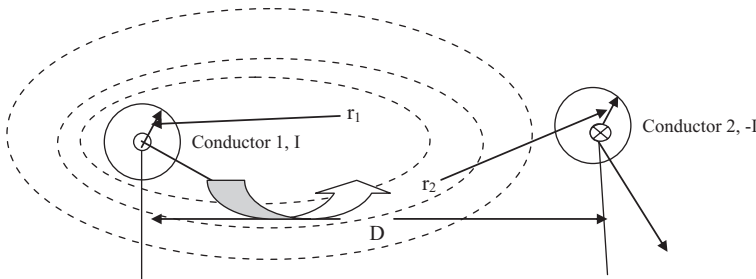$$L_{1,\text{ext}} = 2 \cdot 10^{-7} \ln \frac{D}{r_1} \quad \frac{H}{m}$$ (4.39)

and

FIGURE 4.4
Single-phase two-wire line.

$$L_{1,\text{int}} = \frac{1}{2} \cdot 10^{-7} \quad \frac{\text{H}}{\text{m}} \tag{4.40}$$

which yields the total inductance of this circuit of a single-phase two-wire transmission line as follows.

Total inductance due to current in conductor 1:

$$L_1 = \left(\frac{1}{2} + 2\ln\frac{D}{r_1} \right) \cdot 10^{-7} \quad \frac{\text{H}}{\text{m}} \tag{4.41}$$

$$L_1 = 2 \cdot 10^{-7} \left(\frac{1}{4} + \ln\frac{D}{r_1} \right) \quad \frac{\text{H}}{\text{m}} \tag{4.42}$$

$$\text{using } \ln e^{-1/4} = 1/4$$

yields

$$L_1 = 2 \cdot 10^{-7} \left(\ln e^{-1/4} + \ln\frac{D}{r_1} \right) \quad \frac{\text{H}}{\text{m}} \tag{4.43}$$

$$L_1 = 2 \cdot 10^{-7} \left(\ln\frac{D}{r_1 e^{-1/4}} \right) \quad \frac{\text{H}}{\text{m}} \tag{4.44}$$

$$L_1 = 2 \cdot 10^{-7} \left(\ln\frac{D}{r_1'} \right) \quad \frac{\text{H}}{m}, \text{ where } r_1' = r_1 e^{-1/4} = 0.778 r_1 \tag{4.45}$$

where r_1' is the radius of conductor 1 with no internal flux. The term 0.778 is the modification that yields the new equivalent radius with only external flux.

We can similarly find the conductance due to the current in conductor 2 of (–I) as follows:

$$L_2 = 2 \cdot 10^{-7} \left(\ln\frac{D}{r_2'} \right) \quad \frac{\text{H}}{\text{m}} \tag{4.46}$$

Thus, inductance L for the entire circuit of the single-phase two-wire transmission is given by the sum of Equations 4.45 and 4.46, which yields

$$L = L_1 + L_2 = 2 \cdot 10^{-7} \left(\ln\left(\frac{D^2}{r_1' r_2'} \right) \right)$$

$$L = 4 \cdot 10^{-7} \ln\left(\frac{D}{\sqrt{r_1' r_2'}} \right) \quad \frac{\text{H}}{\text{m}} \tag{4.47}$$

If $r_1' = r_2' = r'$ (i.e., both the conductors belong to the same single-phase two-wire system), then

$$L = 4 \cdot 10^{-7} \ln\left(\frac{D}{r'} \right) \quad \frac{\text{H}}{\text{m}} \tag{4.48}$$

resulting in an inductance per conductor of

$$2 \times 10^{-7} \ln\left(\frac{D}{r'}\right) \quad \frac{\text{H}}{\text{m}} \tag{4.49}$$

We now extend this to an evaluation of multiple conductors in a given circuit, for which we need to find the flux linkages of one conductor in a group, where the sum of the conductor currents is zero (Figure 4.5).

$$\sum_{j=1}^{n} I_j = 0, \text{ for } n \text{ conductors in the group}$$

We can now evaluate step by step the flux linkages of the n conductors at point P as follows:

1. Flux linkages of conductor 1, with radius r_1, due to current I_1, including the internal flux linkages in conductor 1 but excluding all the flux beyond point P at a distance D_{1P}, is given by

$$\Psi_{1P_1} = \left(\frac{I_1}{2} + 2I_1 \ln\frac{D_{1P}}{r_1}\right) \cdot 10^{-7} \quad \text{Wb} - \frac{\text{turn}}{\text{m}} \tag{4.50}$$

$$= 2 \cdot 10^{-7} I_1 \ln\left(\frac{D_{1P}}{r_1'}\right) \quad \text{Wb} - \frac{\text{turn}}{\text{m}} \tag{4.51}$$

2. Flux linkages with conductor 1, with radius r_1, due to current I_2, including the internal flux linkages in conductor 1 but excluding all the flux beyond the point P (i.e., between distance D_{2P} and D_{1P}) is given by

$$\Psi_{1P_2} = \left(\frac{I_2}{2} + 2I_2 \ln\frac{D_{2P}}{D_{12}}\right) \cdot 10^{-7} \quad \text{Wb} - \frac{\text{turn}}{\text{m}} \tag{4.52}$$

$$= 2 \cdot 10^{-7} I_2 \ln\left(\frac{D_{2P}}{D_{12}}\right) \quad \text{Wb} - \frac{\text{turn}}{\text{m}} \tag{4.53}$$
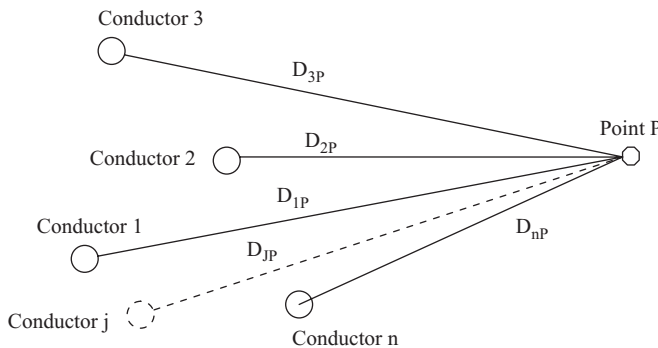

FIGURE 4.5
Circuit with multiple conductors located from point *P*.

3. Therefore, flux linkages Ψ_{1P} with conductor 1, with radius r_1, due to current I_j in all conductors in the group, including the internal flux linkages in conductor j but excluding all the flux beyond point P (i.e. between distance D_{jP} and D_{1P}), is given by

$$\Psi_{1P} = 2 \cdot 10^{-7} \left\{ I_1 \ln\left(\frac{D_{1P}}{r_1'}\right) + I_2 \ln\left(\frac{D_{2P}}{D_{12}}\right) + I_3 \ln\left(\frac{D_{3P}}{D_{13}}\right) + . + .I_n \ln\left(\frac{D_{nP}}{D_{1n}}\right) \right\} \text{Wb} - \frac{\text{turn}}{\text{m}} \quad (4.53)$$

4. Using

$$\sum_{j=1}^{n} I_j = 0$$

we have

$$I_n = -\left(I_1 + I_2 + I_3 + \ldots I_{n-1}\right) \quad (4.54)$$

which yields

$$\Psi_{1P} = 2 \cdot 10^{-7} \left\{ \begin{array}{l} I_1 \ln\left(\frac{1}{r_1'}\right) + I_2 \ln\left(\frac{1}{D_{12}}\right) + I_3 \ln\left(\frac{1}{D_{13}}\right) + . + .I_n \ln\left(\frac{1}{D_{1n}}\right) + \\[3mm] \left\{ \ln\left(\frac{D_{1P}}{D_{nP}}\right) + I_2 \ln\left(\frac{D_{2P}}{D_{nP}}\right) + I_3 \ln\left(\frac{D_{3P}}{D_{nP}}\right) + . + .I_{n-1} \ln\left(\frac{D_{(n-1)P}}{D_{nP}}\right) \right\} \end{array} \right\} \quad (4.55)$$

If we place point P at a far-field location that will assure all flux linkages due to conductor 1 with all other $(n-1)$ conductors, then

$$\frac{D_{1P}}{D_{nP}} = 1; \frac{D_{2P}}{D_{nP}} = 1; \ldots; \frac{D_{(n-1)P}}{D_{nP}} = 1 \quad (4.56)$$

And the factor within braces in Equation 4.55 reduces to zero as $\ln(1) = 0$, yielding

$$\Psi_1 = 2 \cdot 10^{-7} \left\{ I_1 \ln\left(\frac{1}{r_1'}\right) + I_2 \ln\left(\frac{1}{D_{12}}\right) + I_3 \ln\left(\frac{1}{D_{13}}\right) + . + .I_n \ln\left(\frac{1}{D_{1n}}\right) \right\} \quad (4.57)$$

Then the corresponding inductance can be appropriately assessed. Thus, the result in Equation 4.57 can be used to obtain the following inductance for a composite conductor, especially of transmission lines with stranded conductors.

Conductor Y is the return path for conductor X in the transmission line circuit, as can be seen by the currents in each of their sub-parts or strands.

Applying Equation 4.57 to the circuit in Figure 4.6 yields the flux linkages of the strand a, as follows:

$$\Psi_a = 2 \cdot 10^{-7} \frac{I}{n} \left\{ \ln\left(\frac{1}{r_a'}\right) + \ln\left(\frac{1}{D_{ab}}\right) + \ln\left(\frac{1}{D_{ac}}\right) + . + . \ln\left(\frac{1}{D_{an}}\right) \right\}$$
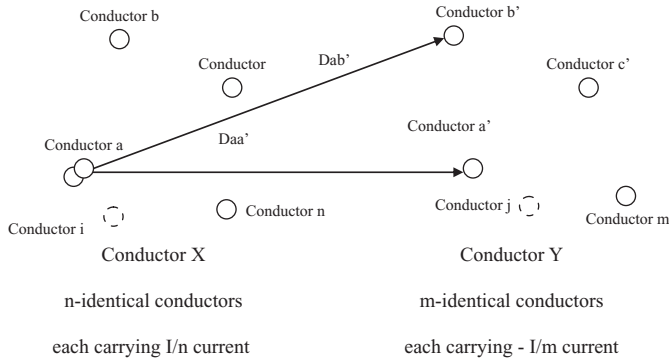
FIGURE 4.6
Transmission line with a composite conductor (stranded conductors).

$$-2\cdot10^{-7}\frac{I}{m}\left\{\ln\left(\frac{1}{D_{aa'}}\right)+\ln\left(\frac{1}{D_{ab'}}\right)+\ln\left(\frac{1}{D_{ac'}}\right)+.+.+\ln\left(\frac{1}{D_{am}}\right)\right\} \tag{4.58}$$

Therefore,

$$\Psi_a = 2\cdot10^{-7}I\ln\frac{\sqrt[m]{D_{aa'}\cdot D_{ab'}\cdot D_{ac'}\cdot....\cdot D_{am}}}{\sqrt[n]{r_a'\cdot D_{ab}\cdot D_{ac}\cdot....\cdot D_{an}}} \quad \text{Wb}-\frac{\text{turn}}{\text{m}} \tag{4.59}$$

which yields

$$L_a = \frac{\Psi_a}{I/n} = 2\cdot n\cdot10^{-7}\cdot\ln\frac{\sqrt[m]{D_{aa'}\cdot D_{ab'}\cdot D_{ac'}\cdot....\cdot D_{am}}}{\sqrt[n]{r_a'\cdot D_{ab}\cdot D_{ac}\cdot....\cdot D_{an}}} \quad \frac{\text{H}}{\text{m}} \tag{4.60}$$

Similarly, for strand *b* of conductor *X*:

$$\Psi_b = 2\cdot10^{-7}I\ln\frac{\sqrt[m]{D_{ba'}\cdot D_{bb'}\cdot D_{bc'}\cdot....\cdot D_{bm}}}{\sqrt[n]{D_{ba}\cdot r_b'\cdot D_{bc}\cdot....\cdot D_{bn}}} \quad \text{Wb}-\frac{\text{turn}}{\text{m}} \tag{4.61}$$

which yields

$$L_b = \frac{\Psi_b}{I/n} = 2\cdot10^{-7}\cdot\ln\frac{\sqrt[m]{D_{ba'}\cdot D_{bb'}\cdot D_{bc'}\cdot....\cdot D_{bm}}}{\sqrt[n]{D_{ba}\cdot r_b'\cdot D_{bc}\cdot....\cdot D_{bn}}} \quad \frac{\text{H}}{\text{m}} \tag{4.62}$$

Therefore, the average inductance of the filaments (strands) of conductors *X* is given by

$$L_{\text{average of }X} = \frac{L_a+L_b+L_c+.+.+L_n}{n} \tag{4.63}$$

For *n* conductors in parallel:

$$L_X = \frac{L_{\text{average of }X}}{n} = \frac{L_a+L_b+L_c+.+.+L_n}{n\cdot n}$$

$$= 2\cdot10^{-7}\cdot\ln\frac{\sqrt[mn]{(D_{aa'}\cdot D_{ab'}\cdot D_{ac'}\cdot....\cdot D_{am})(D_{ba'}\cdot D_{bb'}\cdot D_{bc'}\cdot....\cdot D_{bm})\cdot(\cdot)\cdot(\cdot)..(D_{na'}\cdot D_{nb'}\cdot D_{nc'}\cdot....\cdot D_{nm})}}{\sqrt[n\cdot n]{(D_{aa}\cdot D_{ab}\cdot D_{ac}\cdot....\cdot D_{an})(D_{ba}\cdot D_{bb}\cdot D_{bc}\cdot....\cdot D_{bn})\cdot(\cdot)\cdot(\cdot)..(D_{na}\cdot D_{nb}\cdot D_{nc}\cdot....\cdot D_{nn})}} \quad \frac{\text{H}}{\text{m}}$$

$$\tag{4.64}$$

We will define the parameters as follows:

D_m = numerator; (mn)th root of the $m \times n$ terms: mutual geometric mean distance (GMD) between two conductors

D_s = denominator; n^2 root of n^2 terms: self-GMD of conductor X.

Using these definitions in Equation 4.64 yields the inductance for conductor X:

$$L_X = 2 \cdot 10^{-7} \cdot \ln \frac{D_m}{D_s} \frac{H}{m}$$ (4.65)

which is almost equal to Equation 4.45:

$$L_1 = 2 \cdot 10^{-7} \left(\ln \frac{D}{r_1'} \right) \frac{H}{m}$$

Similarly, using these definitions in Equation 4.64 yields the inductance for conductor Y as follows:

$$L_Y = 2 \cdot 10^{-7} \cdot \ln \frac{D_m}{D_s} \frac{H}{m}$$ (4.66)

and the total inductance of the entire circuit consisting of stranded conductors X and Y, as follows:

$$L = L_X + L_Y$$

Example 4.1

Find the inductance of individual lines as the total inductance of the configuration of conductors A and B, as shown in Figure 4.7, with line B as the return circuit of line A.

SOLUTION 4.1

Note: Change all dimensions to the meter base. Using Equations 4.64 through 4.66 we have $m = n = 3$, and

Line A

Conductors at the corner of an equilateral triangle

of a side of 10 cm;

Radius of conductor 2 cm

Line B

Conductors in a straight line;

conductors are 10 cm apart.

Radius of conductor 2 cm

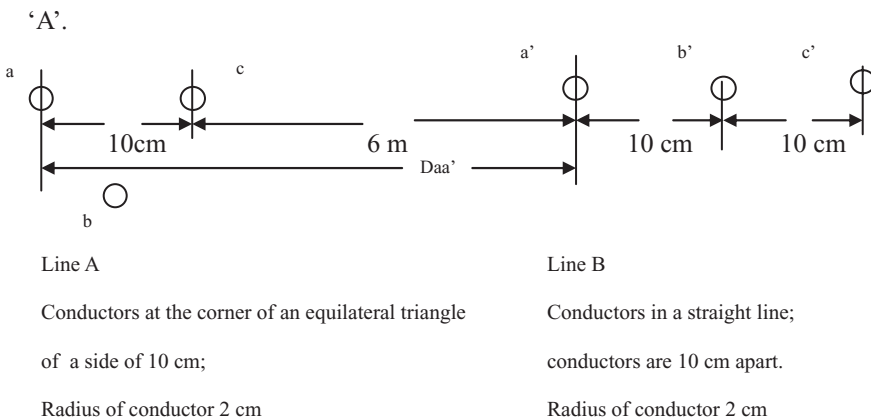**FIGURE 4.7**
Line with stranded conductors: line A and line B as a part of the composite single-phase two-wire transmission line.

$$D_m = \sqrt[9]{\left(D_{aa'} \cdot D_{ab'} \cdot D_{ac'}\right)\left(D_{ba'} \cdot D_{bb'} \cdot D_{bc'}\right)\left(D_{ca'} \cdot D_{cb'} \cdot D_{cc'}\right)}$$

with dimensions as given in Figure 4.7, where, for example, $D_{aa'}$ is the distance between conductor strands a and a', respectively.

$$D_{aa'} = D_{cb'} = 6.1\,\text{m}; \, D_{ab'} = D_{cc'} = 6.2\,\text{m};$$

$$D_{ac'} = 6.3\,\text{m}; \, D_{ca'} = 6\,\text{m}; \, D_{ba'} = 6.05\,\text{m}; \, D_{bb'} = 6.15\,\text{m}; \, D_{bc'} = 6.25\,\text{m}$$

gives

$$D_m = 6.15\,\text{m}$$

$$D_s = \sqrt[9]{\left(D_{aa} \cdot D_{ab} \cdot D_{ac}\right)\left(D_{ab} \cdot D_{ab} \cdot D_{bc}\right)\left(D_{ca} \cdot D_{cb} \cdot D_{cc}\right)}$$

with dimensions as given in Figure 4.7.

$$D_{aa} = D_{bb} = D_{cc} = 0.02\,\text{m} \cdot 0.778 = r'; \, D_{ab} = D_{ac} = D_{ba} = D_{bc} = D_{ca} = D_{cb} = 0.1\,\text{m}$$

gives

$$D_{ms} = 0.0538\,\text{m}$$

gives

$$L_A = 9.48 \cdot 10^{-7} \, \frac{\text{H}}{\text{m}}$$

for line B D_m is the same:

$$D_s = \sqrt[9]{\left(D_{a'a'} \cdot D_{a'b'} \cdot D_{a'c'}\right)\left(D_{a'b'} \cdot D_{a'b'} \cdot D_{b'c'}\right)\left(D_{c'a'} \cdot D_{c'b'} \cdot D_{c'c'}\right)}$$

with dimensions as given in Figure 4.7.

$$D_{a'a'} = D_{b'b'} = D_{c'c'} = 0.02\,\text{m} \cdot 0.778 = r'$$

$$D_{a'b'} = D_{b'c'} = D_{b'a'} = D_{b'c'} = 0.1\,\text{m}; \, D_{a'c'} = D_{c'a'} = 0.2\,\text{m}$$

$$D_s = \sqrt[9]{(0.01556)^3 (0.1)^4 (0.2)^2} = 0.0628\,\text{m}$$

gives

$$L_B = 9.17 \cdot 10^{-7} \, \frac{\text{H}}{\text{m}}$$

Thus,

$$\text{Total } L = L_A + L_B = 18.65 \cdot 10^{-7} \, \frac{\text{H}}{\text{m}}$$

From the inductance of the reactance of the entire transmission line, the circuit comprising lines A and B can be found at a specific frequency f of 60 Hz as follows:

$$X_l = j\omega L = j2\pi f L = j \cdot 2 \cdot \pi \cdot 60 \cdot 18.65 \cdot 10^{-7} = j703.18 \ \text{micro}\,\Omega/\text{m}$$

The values of the inductances at different frequencies can be also found from the library provided by ETAP® for different kinds of conductor sizes and configuration-like stranded conductors.

We now proceed to find the inductance of three-phase lines with symmetrical (equilateral) spacing without neutral, as shown in Figure 4.8.

Three conductors a, b and c of a three-phase line with a GMD of D_s, spaced equally at GMD $= D$, carry currents (without the fourth wire as neutral) as follows:

$$I_a + I_b + I_c = 0 \tag{4.67}$$

Using Equations 4.58 through 4.67, we have

$$\Psi_a = 2 \cdot 10^{-7} \left\{ I_a \ln\left(\frac{1}{D_s}\right) + I_b \ln\left(\frac{1}{D}\right) + I_c \ln\left(\frac{1}{D}\right) \right\} \quad \text{Wb} - \frac{\text{turn}}{\text{m}} \tag{4.68}$$

Using Equation 4.67 in Equation 4.68 yields

$$\Psi_a = 2 \cdot 10^{-7} \left\{ I_a \ln\left(\frac{1}{D_s}\right) - I_a \ln\left(\frac{1}{D}\right) \right\} \quad \text{Wb} - \frac{\text{turn}}{\text{m}} \tag{4.69}$$

which yields the inductance per phase of a three-phase line as

$$L_a = L_b = L_c = 2 \cdot 10^{-7} \left\{ \ln\left(\frac{D}{D_s}\right) \right\} \frac{\text{H}}{\text{m}} \tag{4.70}$$

We now proceed to find the inductance of three-phase lines with unsymmetrical spacing without neutral, as shown in Figure 4.9.

1. Here, because of the unsymmetrical spacing between lines, as shown in Figure 4.9 with distances D_{12}, D_{23} and D_{31}, between conductors a and c, conductors c and b and conductors b and c, respectively, the flux linkages and inductance of each phase are not the same.
2. This unsymmetrical spacing leads to an unbalanced circuit from start to finish as the 'crow flies' in distance or the length of each conductor.
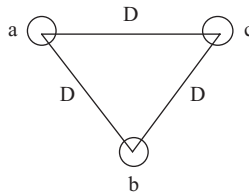

FIGURE 4.8
Three-phase line with equilateral spacing of distance D, without neutral.
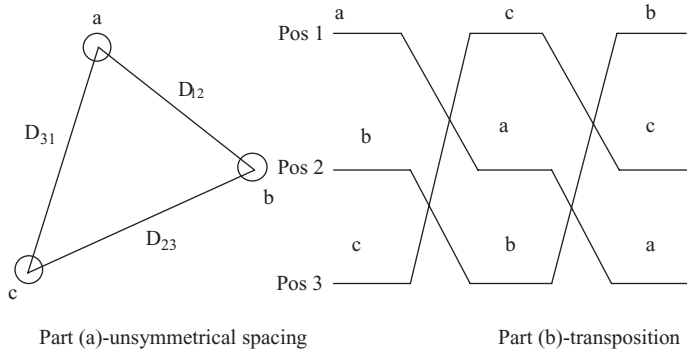
FIGURE 4.9
Three-phase transmission line with unsymmetrical spacing and transposition of conductor positions.

3. This imbalance is restored by exchanging or transposing the physical positions of the conductors at regular intervals over equal distances from start to finish, as shown in Figure 4.9b.

4. Thus, at different distances and positions, the average inductance of one conductor of a transposed line needs to be calculated as follows:

Step 1:

Conductor *a*: position 1; conductor *b*: position 2; conductor *c*: position 3

$$\Psi_{a1} = 2 \cdot 10^{-7} \left\{ I_a \ln\left(\frac{1}{D_s}\right) + I_b \ln\left(\frac{1}{D_{12}}\right) + I_c \ln\left(\frac{1}{D_{31}}\right) \right\} \quad \text{Wb} - \frac{\text{turn}}{\text{m}} \tag{4.71}$$

Step 2:

Conductor *a*: position 2; conductor *b*: position 3; conductor *c*: position 1

$$\Psi_{a2} = 2 \cdot 10^{-7} \left\{ I_a \ln\left(\frac{1}{D_s}\right) + I_b \ln\left(\frac{1}{D_{23}}\right) + I_c \ln\left(\frac{1}{D_{12}}\right) \right\} \quad \text{Wb} - \frac{\text{turn}}{\text{m}} \tag{4.72}$$

Step 3:

Conductor *a*: position 3; conductor *b*: position 1; conductor *c*: position 2

$$\Psi_{a3} = 2 \cdot 10^{-7} \left\{ I_a \ln\left(\frac{1}{D_s}\right) + I_b \ln\left(\frac{1}{D_{31}}\right) + I_c \ln\left(\frac{1}{D_{23}}\right) \right\} \quad \text{Wb} - \frac{\text{turn}}{\text{m}} \tag{4.73}$$

This results in an average value of the total flux linkage for line *a* as follows:

$$\Psi_a = \frac{\Psi_{a1} + \Psi_{a2} + \Psi_{a3}}{3}$$

$$= 2 \cdot 10^{-7} \left\{ 3I_a \ln\left(\frac{1}{D_s}\right) + I_b \ln\left(\frac{1}{D_{12}D_{23}D_{31}}\right) + I_c \ln\left(\frac{1}{D_{31}D_{12}D_{23}}\right) \right\} \quad \text{Wb} - \frac{\text{turn}}{\text{m}} \tag{4.74}$$